CRYSTAL GROWTH & DESIGN

pubs.acs.org/crystal

Article

Investigating the Role of Weak Interactions to Explore the Polymorphic Diversity in Difluorinated Isomeric *N*-Phenylcinnamamides

Rohit Bhowal* and Deepak Chopra*

Cite This: *Cryst. Growth Des.* 2021, 21, 4162−4177

Read Online

ACCESS | Metrics & More | Article Recommendations | Supporting Information

ABSTRACT: A total of nine difluoro derivatives of *N*-phenylcinnamamides have been synthesized from fluoro-substituted cinnamic acids and anilines in order to investigate the formation of polymorphs arising due to the conformational flexibility around the amide and vinyl group. Among them, four compounds have been found to exist in multiple polymorphic forms, which includes concomitant polymorphism, solvatomorphism, and packing polymorphism, while the remaining five compounds display monomorphic behavior. Crystal structure analyses of all the forms belonging to these four compounds reveal that, although the molecules are primarily held by strong N−H···O hydrogen bonds, the relative interplay of weak C−H···F, C−H···O, C−H···π, and π···π interactions allows the flexible molecules to adopt different orientations and exhibit polymorphism. These forms interestingly also display different thermal stabilities, and they have been quantified by intermolecular interaction topological analyses. The occurrence of different primary packing motifs in these crystal structures has been further investigated by the crystal structure prediction (CSP) computational method, wherein an energy landscape of an unsubstituted *N*-phenylcinnamamide was generated and a number of hypothetical structures were accessed with experimentally obtained crystal structures of its difluoro-substituted derivatives.

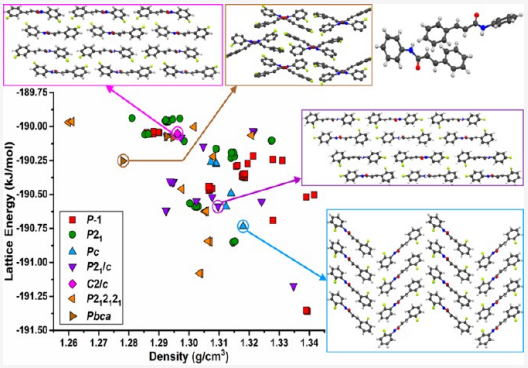

1. INTRODUCTION

Fluorine chemistry[1−3] has experienced an exponential growth, from representing a small subfield of organic chemistry into a major area of multidisciplinary research of drug design that involves health and food industries.[4−7] The previous few decades have witnessed the evolution of fluorine substitution as one of the structural trends in the world of medicinal chemistry, where nearly 50% of all the blockbuster drug molecules contain fluorine atoms.[8−12] Peptide/protein engineering relies on structure tailoring of fluorinated amino acids and their subsequent tactical amalgamation into the peptide chain in order to achieve a three-dimensional view of peptide−receptor interactions.[13−15] The possibility of obtaining polymorphism and pseudopolymorphism is quite high among active pharmaceutical ingredients, and this phenomenon can be considered either a blessing or a nuisance in different stages of drug design, as it might have direct medical implications.[16−21] The term "polymorphs" include those crystal systems in which a substance can crystallize in multiple crystal structures having different unit cell parameters, where each form displays the same empirical formula.[22−25] Solvatomorphs or pseudopolymorphs, on the other hand, include crystal systems with different unit cell parameters, where the unit cells differ in their elemental composition only through the inclusion of one or more solvent molecules.[26−28] Concomitant polymorphs are defined as the simultaneous crystallization of two or more forms due to their concurrent nucleation, and their formation is controlled by both the kinetics of crystallization and thermodynamics of crystal packing.[29−31] Packing polymorphs include crystal systems having similar molecular conformations, differing only in the arrangement of molecules in their crystal packing environment.[32−34] The polymorphic forms of a drug may exhibit distinct solid-state physicochemical properties such as intrinsic dissolution rate,[35,36] solubility,[37] tabletability,[38,39] thermal stability,[40] flowability,[41] hygroscopicity,[42,43] etc. and also various drug outcomes such as drug efficacy,[44] bioavailability,[45] and toxicity.[46,47] Hence, it is of prime importance to conduct an in-depth exploration into the polymorphic possibility of different drugs and their precursors using both experimental techniques and computational interpretations, which is one of the principal aims of crystal engineering research.

Polymorphism was first discovered in benzamide by Wöhler and von Liebig in 1832,[48] and since then remarkable progress

Received: April 12, 2021
Revised: June 9, 2021
Published: June 25, 2021

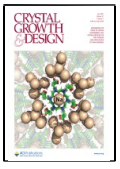

https://doi.org/10.1021/acs.cgd.1c00422
Cryst. Growth Des. 2021, 21, 4162−4177

toward the discovery of new polymorphs of organic materials has been accomplished. As a part of a continuous endeavor to appreciate the solid-state diversity present in *N*-phenylbenzamides,[49−51] herein we have further extended our study to explore the polymorphic possibilities in the difluoro-substituted *N*-phenylcinnamamides. A recent survey of cinnamamide molecules in the Cambridge Structural Database (CSD)[52] has yielded only 30 hits, out of which only 3 molecules were *N*-phenylcinnamamide derivatives, and no structures exhibited any polymorphic behavior. The molecular framework of cinnamamide derivatives has been integrated into numerous biologically active synthetic compounds, since it promotes both hydrophobic and hydrogen-bonding interactions originating from the phenyl ring and the amide group, respectively, highly suitable for interacting with the molecular target. By introduction of a C−F group, also termed as "organic fluorine",[53,54] it is expected to exhibit poor hydrogen bond acceptor properties, which can be attributed to the weak polarizability of fluorine atoms[55,56] and is expected to embrace weak C−H···F interactions. In order to quantitatively assess the support provided by weak noncovalent interactions originating from organic fluorine in the presence of strong N−H···O and moderately strong C−H···O and C−H···π hydrogen bonds, we have performed the synthesis and crystallization of a series of nine isomeric difluorinated *N*-phenylcinnamamides (Scheme 1), out of which four compounds crystallized in multiple

Scheme 1. Synthetic Route and Chemical Structures of *N*-Phenylcinnamamide (ADB) and Its Difluoro-Substituted Analogues

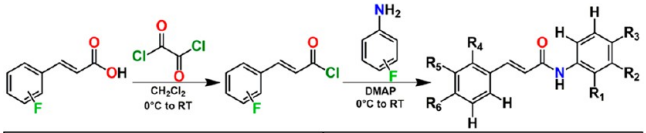

ADB: R_1=R_2=R_3=R_4=R_5=R_6=H	3ADB3: R_2=R_5=F, R_1=R_3=R_4=R_6=H
2ADB2: R_1=R_4=F, R_2=R_3=R_5=R_6=H	3ADB4: R_2=R_6=F, R_1=R_3=R_4=R_5=H
2ADB3: R_1=R_5=F, R_2=R_3=R_4=R_6=H	4ADB2: R_3=R_4=F, R_1=R_2=R_5=R_6=H
2ADB4: R_1=R_6=F, R_2=R_3=R_4=R_5=H	4ADB3: R_3=R_5=F, R_1=R_2=R_4=R_6=H
3ADB2: R_2=R_4=F, R_1=R_3=R_5=R_6=H	4ADB4: R_3=R_6=F, R_1=R_2=R_4=R_5=H

polymorphic forms. A subtle interplay of strong hydrogen bonds and weak intermolecular interactions sometimes involving disordered fluorine, arising from the conformational flexibility of the difluorinated phenyl rings, has been found to exert a substantial effect on the thermal stabilities of these polymorphs. The occurrence of polymorphic forms of a molecule provides the opportunity to investigate its structural landscape from experimentally determined crystal structures.[57] However, it is practically an uphill task to obtain all of the plausible structures in the landscape from crystallization experiments alone; hence, the miscellaneous crystal packing plausibilities of *N*-phenylcinnamamides have been computed by employing the computational CSP method within a small energy space via a crystal lattice energy vs density plot.[58] Predicting crystal structures of an organic molecule from its molecular structure alone is of considerable industrial importance. This is a highly complicated venture due to the number of degrees of freedom to be explored and the complexities arising from inter- and intramolecular interactions, especially in our compound of interest, which has high flexibility.[59] One of the major disadvantages of this CSP method is that it does not take into account the kinetic factors such as nucleation dynamics, solvent effects, temperature, pressure, and humidity affecting the crystallization pathway and hence sometimes fails to predict experimentally obtained crystal structures. An examination of strong and weak intermolecular interactions via an energy framework analysis would lead to a better understanding and comparison of the crystal packing modes in polymorphic systems.

2. RESULTS AND DISCUSSION

In this investigation we have synthesized *N*-phenylcinnamamide (ADB) and a library of nine difluoro-substituted ADB molecules (see Scheme 1), which contain an amide group and a double bond bridging two phenyl rings connected to organic fluorine, so as to observe the occurrence of C−H···F−C(sp^2) and related weak intermolecular interactions acting in conjunction with strong N−H···O=C hydrogen bonds. Synthetic procedures and purification methods for the compounds are provided in detail in the Supporting Information. The bulk compounds were crystallized in a wide range of solvents and solvent mixtures (for details see Table S1) and were characterized by single-crystal X-ray diffraction (SCXRD) experiments, which allowed the identification of intermolecular interactions and molecular self-assembly in the solid state. An extensive screening by crystallization experiments of the unsubstituted and difluoro-substituted molecules in the series has yielded three polymorphic forms of 2ADB4 (forms I−III), one solvatomorph (form I), and two polymorphs of 3ADB3 (forms II and III), two concomitant polymorphs of 4ADB2 (forms I and II) and two packing polymorphs of 4ADB4 (forms I and II) (see Table S2). A closer inspection of the molecular structures in the series revealed significant differences in their geometrical features (See Tables 1 and 2). The thermal stabilities of the compounds were determined by differential scanning calorimetry (DSC) experiments, and it was found that each polymorph displayed a quite distinct melting point, indicating the pivotal role of cooperative noncovalent interactions. First, we have focused on only those compounds that exhibited polymorphic behavior, and hence a

Table 1. Torsion Angles (deg) for 2ADB2, 2ADB3, 3ADB2, and Three Forms of 2ADB4 and 3ADB3 Each

			2ADB4				3ADB3		
	2ADB2	2ADB3	form I	form II	form III	3ADB2	form I	form II	form III
C7−N1−C1−C6	39.81(4)	−34.35(6)	51.27(2)	39.19(3)	51.64(2)	155.02(10)	−171.95(2)	−42.50(2)	−145.06(3)
C8−C9−C10−C11	150.22(3)	21.37(7)	9.31(2)	152.26(2)	8.37(3)	−158.27(11)	−6.05(3)	161.79(6)	8.80(6)
C22−N2−C16−C21		−26.54(6)	48.58(2)		51.61(2)				−22.63(5)
C23−C24−C25−C26		−165.33(4)	12.84(2)		13.33(3)				170.79(4)
(C1−C6)/(C10−C15)interplanar angle	4.2	2.3	76.2	4.1	75.0	13.1	5.7	75.3	28.2
(C16−C21)/(C25−C30) interplanar angle		4.3	76.2		78.9				25.1

https://doi.org/10.1021/acs.cgd.1c00422
Cryst. Growth Des. 2021, 21, 4162−4177

Table 2. Torsion Angles (deg) for 3ADB4, 4ADB3, and Two Polymorphs of 4ADB2 and 4ADB4 Each along with Unsubstituted ADB

		4ADB2			4ADB4		
	3ADB4	form I	form II	4ADB3	form I	form II	ADB
C7−N1−C1−C6	−159.96(16)	−41.38(13)	−140.93(12)	−155.67(12)	−161.59(12)	−156.14(16)	−20.25(6)
C8−C9−C10−C11	−17.66(3)	160.39(13)	153.24(17)	168.87(12)	170.51(13)	−18.17(3)	−6.34(7)
C22−N2−C16−C21							−40.84(5)
C23−C24−C25−C26							−7.52(6)
(C1−C6)/(C10−C15) interplanar angle	16.8	73.7	2.4	7.6	4.5	12.7	24.5
(C16−C21)/(C25−C30) interplanar angle							40.3

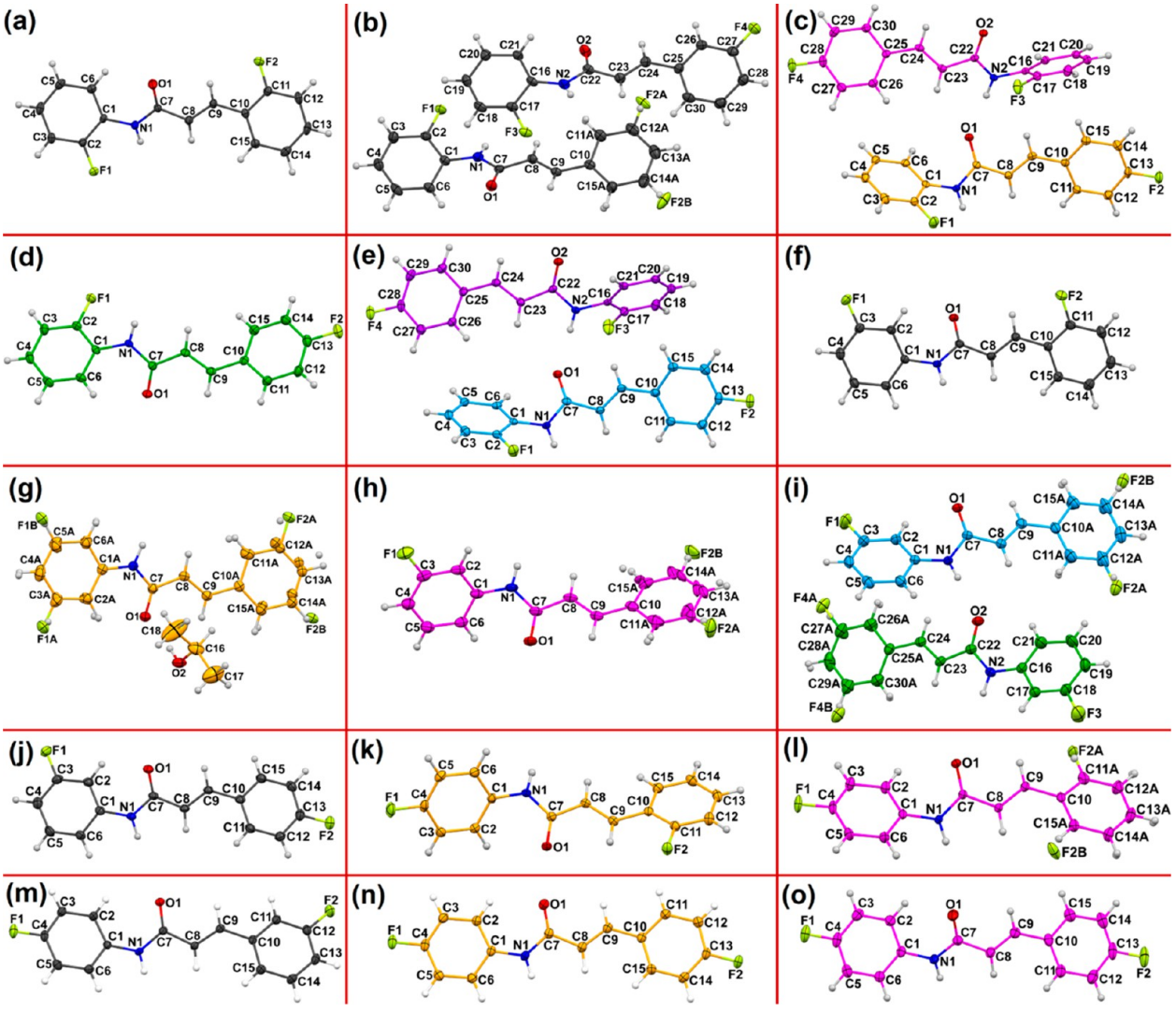

Figure 1. ORTEP drawings of (a) 2ADB2, (b) 2ADB3, (c) form I of 2ADB4 (orange-magenta), (d) form II of 2ADB4 (green), (e) form III of 2ADB4 (blue-purple), (f) 3ADB2, (g) form I of 3ADB3 (orange), (h) form II of 3ADB3 (magenta), (i) form III of 3ADB3 (blue-green), (j) 3ADB4, (k) form I of 4ADB2 (orange), (l) form II of 4ADB2 (magenta), (m) 4ADB3, (n) form I of 4ADB4 (orange), and (o) form II of 4ADB4 (magenta), drawn with 50% ellipsoidal probability with the atom-numbering schemes. Different colors of carbon atoms represent the symmetry-independent positions of molecules in the asymmetric unit in the polymorphs.

total of 10 new structures have been discussed in terms of their conformational preferences and adaptation of complementary supramolecular domains supported by an energetic quantification of the intermolecular interaction topology. Thereafter, we have also investigated the occurrence of isostructurality and isomorphism[60,61] in the entire family of difluorinated ADB molecules, followed by an in-depth analysis of the occurrence of different supramolecular motifs in the crystal structure landscape of the unsubstituted compound. This is compared with the observed motifs in the different polymorphs of the substituted crystal structures, which constitutes a general topological interaction landscape via the technique of crystal structure prediction.[62]

2.1. Polymorphs of 2ADB4: Forms I−III. *2.1.1. Molecular Packing.* 2ADB4 crystallizes in three polymorphic forms, where its first form (form I) crystallizes in the triclinic crystal system

https://doi.org/10.1021/acs.cgd.1c00422
Cryst. Growth Des. 2021, 21, 4162−4177

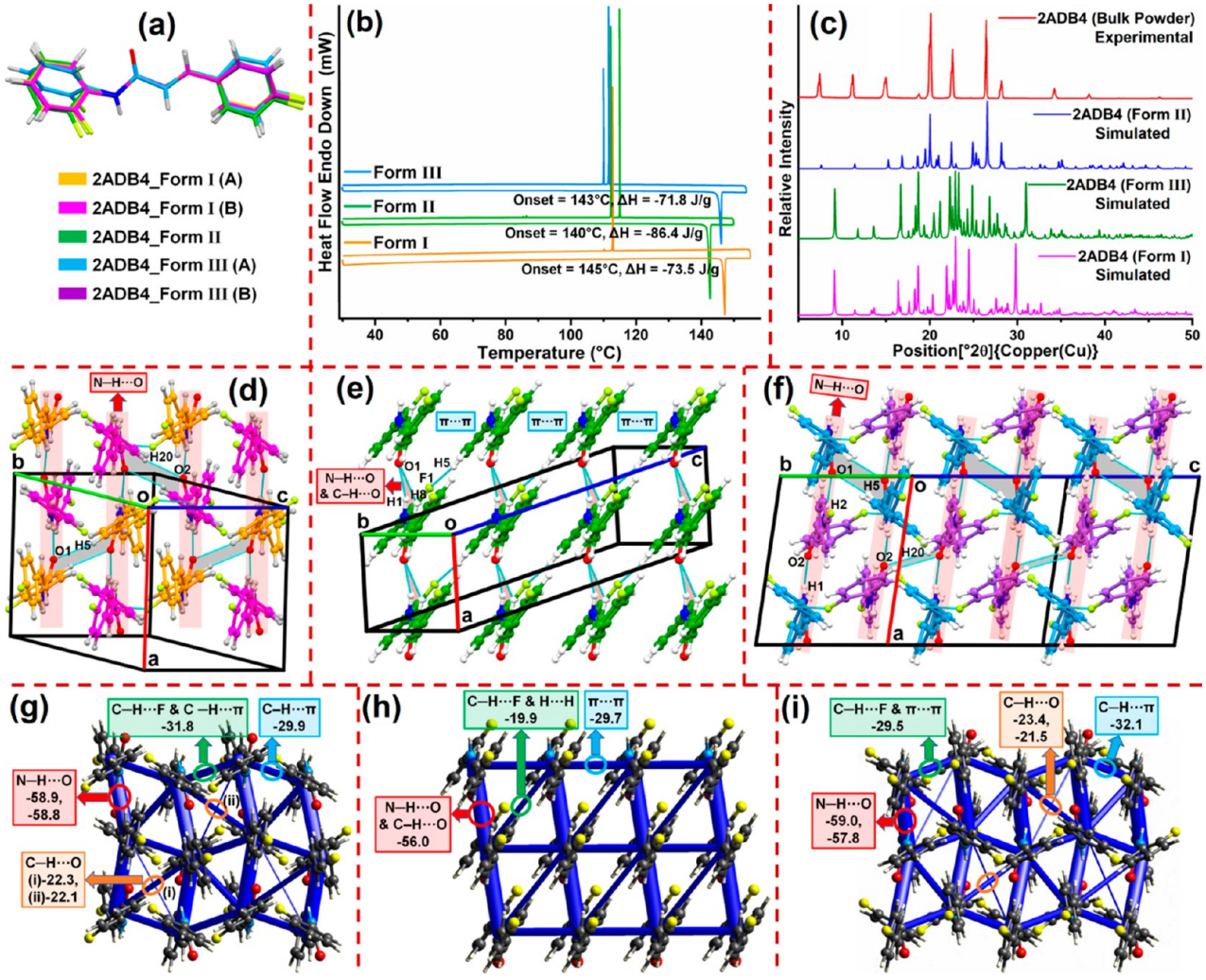

Figure 2. (a) Molecular overlay of five symmetry-independent molecules (two, one, and two molecules from forms I–III of 2ADB4, respectively) at the solid-state geometry. (b) DSC profiles of the three polymorphs of 2ADB4 at 3 °C/min of a heating–cooling cycle. (c) Overlay of experimental PXRD patterns of 2ADB4 bulk powder and the simulated patterns of the three polymorphs. Crystal structure projections of (d) 2ADB4 (form I), (e) 2ADB4 (form II), and (f) 2ADB4 (form III) at 100 K. Energy frameworks for (g) 2ADB4 (form I), (h) 2ADB4 (form II), and (i) 2ADB4 (form III), representing the total interaction energies in kJ/mol.

with centrosymmetric space group $P\bar{1}$ and having two molecules (orange-magenta) in the asymmetric unit ($Z' = 2$) (Figure 1c). The symmetry-independent molecules form a three-dimensional molecular sheet along the *ac* plane, connected via highly directional N1–H1···O2═C22 and N2–H2···O1═C7 hydrogen bonds (red bands in Figure 2d) along the *a* axis and weaker C19–H19···F4 and bifurcated C4/C27–H4/H27···F2 interactions along the *c* axis (Figure S2a). The molecules in form I are further bound by C20–H20···O2═C22 and C5–H5···O1═C7 $R_2^2(14)$ hydrogen bond synthons, both related by inversion centers, which diagonally link the N–H···O hydrogen-bonded molecular chains (gray bands in Figure 2d). The second form (form II) of 2ADB4 crystallizes in the monoclinic crystal system with noncentrosymmetric space group $P2_1$ having one molecule (green) in its asymmetric unit ($Z' = 1$) (Figure 1d). The molecules are primarily held by bifurcated N1/C8–H1/H8···O1═C7 $_2^1R(6)$ hydrogen bond synthons down the *a* axis (red zones in Figure 2e and Figure S2b), while successive molecular chains are bridged via C3–H3···F1 and C12–H12···F2 interactions along the *c* axis (Figure S2b). The phenyl rings in form II are almost coplanar with each other (2ADB4 form II in Table 1), which helps in the promotion of $\pi\cdots\pi$ interactions between the aromatic rings in addition to C5–H5···F1 interactions (Figure 2e). The third form (form III) of 2ADB4 crystallizes in the monoclinic crystal system with centrosymmetric space group $P2_1/c$ having two molecules (blue-purple) in the asymmetric unit ($Z' = 2$) (Figure 1e) linked by highly directional N1–H1···O2═C22 and N2–H2···O1═C7 hydrogen bonds down the *a* axis (red bands in Figure 2f). These molecular columns are diagonally bridged via C5–H5···O1═C7 and C20–H20···O2═C22 $R_2^2(14)$ hydrogen bond synthons (gray bands in Figure 2f). The crystal packing in a view along the *bc* plane exhibits a wavelike zigzag orientation of molecules promoted by C20–H20···F1, C3–H3···F4, C18–H18···F2, and C4–H4···F2 interactions (Figure S2c).

2.1.2. Thermal and PXRD Analyses. DSC experiments of all the polymorphic forms of 2ADB4 were performed to unravel their relative thermal stabilities (Figure 2b). All three forms displayed smooth endotherms with sharp melting peaks, where form I was found to exhibit the highest thermal stability with a melting point at 145 °C ($\Delta H = -73.5$ J/g) (orange line in Figure 2b), followed by form III, which melts at 143 °C ($\Delta H = -71.8$ J/

https://doi.org/10.1021/acs.cgd.1c00422
Cryst. Growth Des. 2021, 21, 4162–4177

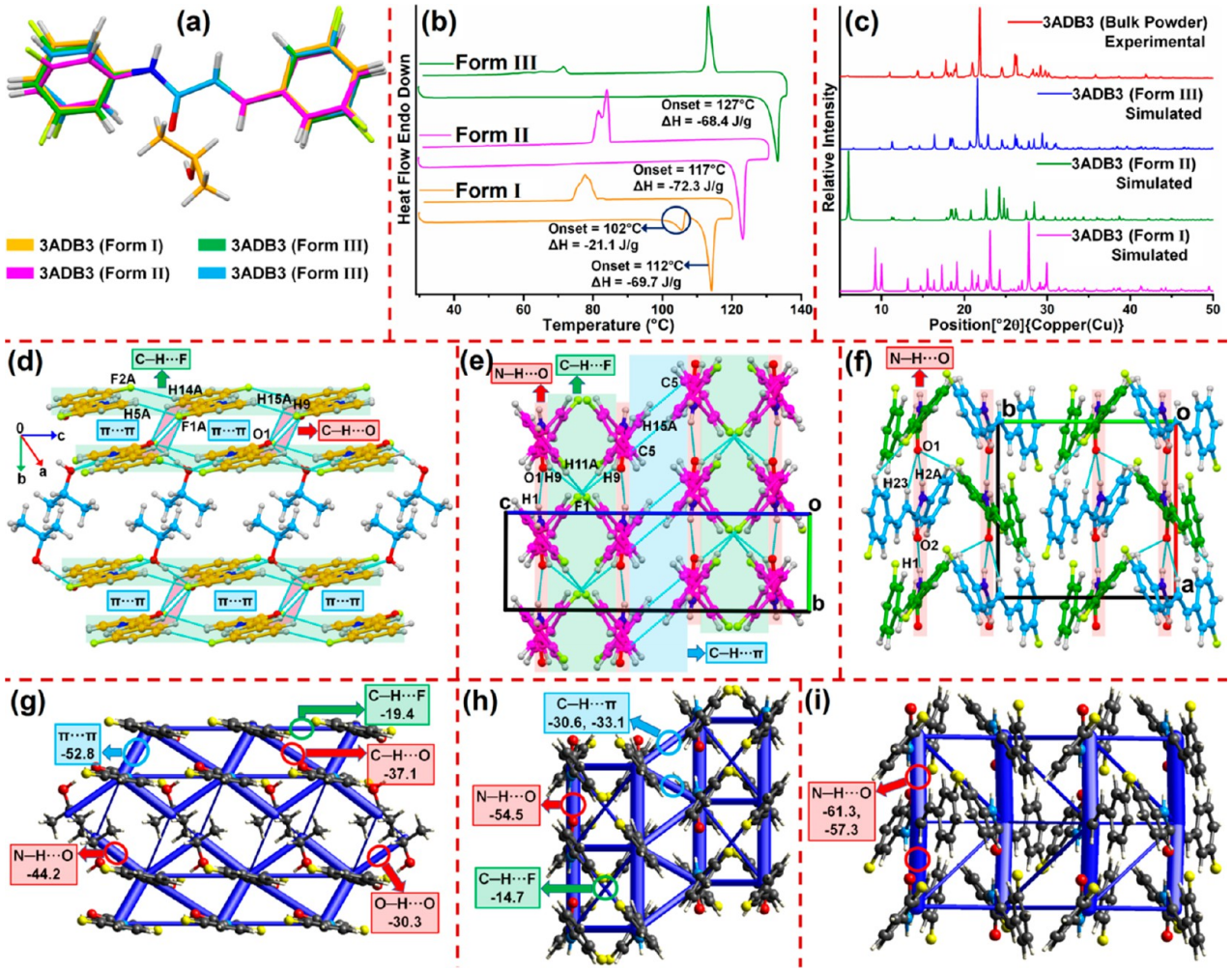

Figure 3. (a) Molecular overlay of four symmetry-independent molecules (one, one, and two molecules from forms I–III of 3ADB3 respectively) at the solid-state geometry. (b) DSC profiles of the three polymorphs of 3ADB3 at 3 °C/min of a heating–cooling cycle, (c) Overlay of PXRD patterns of 3ADB3 bulk powder and the simulated patterns of their three polymorphs. Crystal structure projections of (d) 3ADB3 (form I), (e) 3ADB3 (form II), and (f) 3ADB3 (form III) at 100 K. Energy frameworks for (g) 3ADB3 (form I), (h) 3ADB3 (form II), and (i) 3ADB3 (form III), representing the total interaction energies in kJ/mol.

g) (blue line in Figure 2b) and finally form II exhibiting the lowest thermal stability with a melting point at 140 °C (ΔH = −86.4 J/g) (green line in Figure 2b). The relative differences in melting points of the three forms can be explained by an energy framework analysis of their respective IEs. Form I exhibits the highest thermal stability due to the presence of a strong network of electrostatically dominated N–H···O (IE = −58.9, −58.8 kJ/mol), C–H···F and C–H···π (IE = −31.8 kJ/mol), and C–H···O (IE = −29.9, −22.4 kJ/mol) interactions (Figure 2g). On the other hand, form III displays a comparatively lower melting point, evidently due to the slightly lower values of IEs in molecular dimers connected by N–H···O (IE = −59.0, −57.8 kJ/mol), C–H···F and C–H···π (IE = −29.5 kJ/mol), and C–H···O (IE = −23.1, −21.5 kJ/mol) interactions (Figure 2i). Finally, the lowest thermal stability of form II can be elucidated from the much lower values of IEs in dimers linked via bifurcated N–H···O and C–H···O hydrogen bonds represented by vertical tubes (IE = −56.0 kJ/mol) and supported by C–H···F and H···H interactions represented by the diagonal tubes (IE = −19.9 kJ/mol) (Figure 2h). The experimental powder pattern of the bulk powder of 2ADB4 has been compared with the simulated PXRD patterns of all the polymorphic forms, and it shows that the bulk powder is a representative of form II (Figure 2c). This has been further proved using the powder profile fitting refinement technique, where only form II yielded satisfactory results (Figure S9a).

2.2. Polymorphs of 3ADB3: Forms I–III. *2.2.1. Molecular Packing.* 3ADB3 crystallizes in three polymorphic forms, where form I is a solvatomorph crystallizing in the triclinic crystal system with the centrosymmetric space group $P\bar{1}$ having one 3ADB3 molecule and an isopropyl alcohol solvent molecule in the asymmetric unit (Figure 1g). Both 3-fluorobenzene rings experience orientational disorder (sof of F1A = 0.865(2), sof of F1B = 0.135(2), sof of F2A = 0.910(2), sof of F2B = 0.090(2), where sof stands for site occupancy factor) and maintain a coplanar orientation with respect to each other (3ADB3 (form I) in Table 1), which assists in the formation of two-dimensional molecular layers via C5A–H5A···F1A and C14A–H14A···F2A interactions along the *a* axis (green belts in Figure 3d) and via a C13A–H13A···F2A $R_2^2(8)$ hydrogen bond synthon related by an inversion center along the *c* axis (Figure S3a). These successive molecular sheets are further stabilized by bifurcated C15A/C9–H15A/H9···O1 $R_2^1(6)$ hydrogen bonds (red bands in Figure 3d) and π··π interactions down the *b* axis (blue bands

https://doi.org/10.1021/acs.cgd.1c00422
Cryst. Growth Des. 2021, 21, 4162–4177

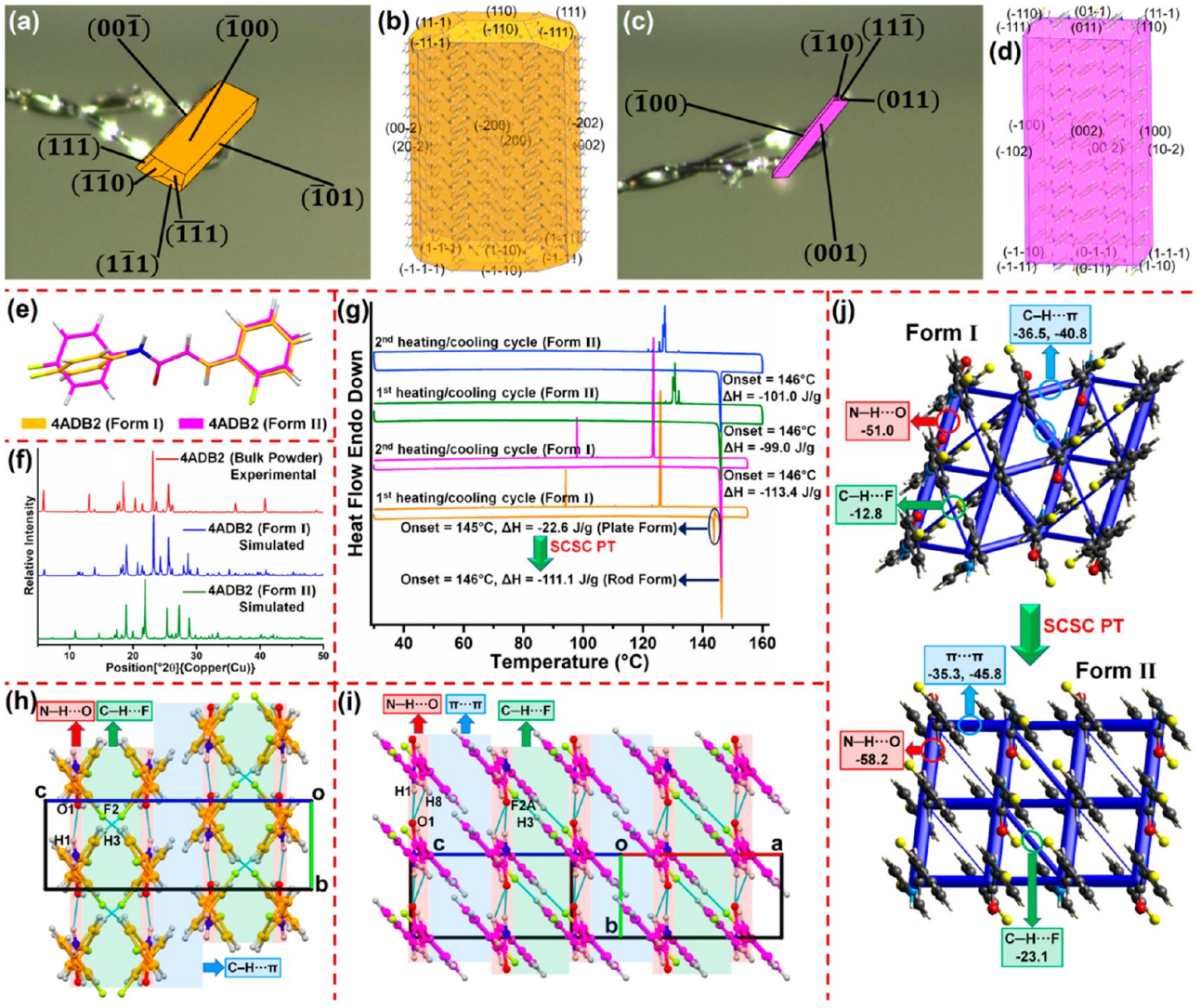

Figure 4. (a) Face indexation for form I of 4ADB2 and (b) prediction of morphology for form I of 4ADB2 from BFDH calculations.[63−65] (c) Face indexation for form II of 4ADB2 and (d) prediction of morphology for form II of 4ADB2 from BFDH calculations. (e) Molecular overlay of two symmetry-independent molecules (one molecule each from forms I and II of 4ADB2) atthe solid-state geometry. (f) Overlay of the PXRD pattern of 4ADB2 bulk powder with the simulated patterns of their concomitant polymorphs. (g) DSC profiles for the two forms of 4ADB2 at 3 °C/min for two heating−cooling cycles. Crystal projections of (h) 4ADB2 (form I) along the *bc* plane and (i) 4ADB2 (form II) along the *b* axis at 100 K. (j) The structural transition from form I to form II in 4ADB2 explained by an energy framework analysis representing their total interaction energies in kJ/mol.

in Figure 3d). The isopropyl alcohol molecules (demarcated in blue in Figure 3d) bridge the stacked molecular layers via an $R_2^1(6)$ bifurcated N1/C8−H1/H8···O2 hydrogen bond synthon and O2−H2···O1═C hydrogen bonds (Figure S3a). Form II crystallizes in the monoclinic crystal system with centrosymmetric space group $C2/c$ having one molecule (magenta) in the asymmetric unit ($Z' = 1$) (Figure 1h). The molecules are primarily held by N1−H1···O1 hydrogen bonds along the *b* axis (red belts, Figure 3e), while the oppositely tilted orientation of both phenyl rings (3ADB3 (form II) in Table 1) allows alternate regions of $R_2^1(6)$ bifurcated C9/C11A−H9/H11A···F1 hydrogen bond synthons related by the 2-fold axis (green belts in Figure 3e and Figure S3b) and C15A−H15A···C5(π) interactions related by an inversion center (blue belts in Figure 3e and Figure S3b). The 3-fluorobenzene ring on the vinyl end experiences orientational disorder (sof of F2A = 0.540(3), sof of F2B = 0.460(3)), which assists in the propagation of molecules along the *a* axis and is facilitated by C4−H4···F2A hydrogen bonds (Figure 3e). Form III crystallizes in the orthorhombic crystal system with the noncentrosymmetric space group $P2_12_12_1$ having two molecules (blue-green) in the asymmetric unit (Figure 1i), which are primarily held by an alternating combination of highly directional N1−H1···O2═C22 and bifurcated N2/C23−H2A/H23···O1═C7 $R_2^1(6)$ hydrogen bond synthons down the *a* axis through the 2_1 screw axis (red bands in Figure 3f and Figure S3c). Interestingly here also, the 3-fluorobenzene rings on the vinyl end of both symmetry-independent molecules experience orientational disorder (sof of F2A = 0.890(3), sof of F2B = 0.110(3), sof of F4A = 0.890(3), sof of F4B = 0.110(3)), which promotes the propagation of molecules along the *c* axis and occurs via 2_1 screw axes facilitated by C4−H4···F2A and bifurcated C20−H20···F2A/F4A interactions (Figure S3c).

2.2.2. Thermal and PXRD Analyses. DSC experiments have revealed that the polymorphs of 3ADB3 have quite divergent thermal stabilities; these have been justified from an analysis of their energy frameworks (Figure 3b). The DSC thermogram of

https://doi.org/10.1021/acs.cgd.1c00422
Cryst. Growth Des. 2021, 21, 4162−4177

form I shows the expulsion of solvent isopropyl alcohol molecules from its crystal lattice by a small endothermic peak at 102 °C (ΔH = −21.1 J/g), followed by its melting indicated by a sharp endothermic peak at 112 °C (ΔH = −69.7 J/g) (orange line in Figure 3b). The DSC profile of form II exhibits a comparatively higher melting point with an endothermic peak at 117 °C (ΔH = −72.3 J/g) (magenta line in Figure 3b), while form III displays the highest thermal stability with a melting peak at 127 °C (ΔH = −68.4 J/g) (green line in Figure 3b). The lowest thermal stability of form I can be explained by the lower values of IEs in molecules connected by N−H···O (IE = −44.2 kJ/mol, Figure 3g) and O−H···O hydrogen bonds (−30.3 kJ/mol, Figure 3g), which bind the guest isopropyl alcohol with the host molecules; hence, it melts immediately after solvent expulsion. In contrast, the higher thermal stability of form II is due to dimers connected by relatively stronger N−H···O hydrogen bonds represented by vertical tubes (IE = −54.5 kJ/mol, Figure 3h). The highest thermal stability of form III can be justified by dimers linked by the strongest N−H···O hydrogen bonds represented by vertical tubes (IE = −61.3, −57.3 kJ/mol, Figure 3i). A comparison of experimental PXRD patterns of the 3ADB3 bulk powder with the simulated PXRD patterns of its polymorphs shows us that the bulk powder is representative of its thermally most stable polymorph, form III (Figure 3c), which has been validated from a profile fitting refinement, where only form III yielded satisfactory results (Figure S9b).

2.3. Polymorphs of 4ADB2: Forms I and II. *2.3.1. Molecular Packing.* 4ADB2 crystallizes concomitantly in two polymorphic forms, where form I has a plate morphology (4ADB2 in Figure S1), and it crystallizes in the monoclinic crystal system with the centrosymmetric space group $C2/c$ having one molecule in the asymmetric unit (Z' = 1, Figure 1k). The molecules are primarily held by N1−H1···O1═C7 hydrogen bonds down the b axis (red belts in Figure 4h). These molecular chains connected by N−H···O hydrogen bonds in a view along the ac plane are found to be interlinked by distinct alternate layers of C3−H3···F2, and C12−H12···F1 interactions (green layers in Figure S4a) and C15−H15···C5/C6(π), C5−H5···C15(π), and C6−H6···C9(π) interactions (blue belts in Figure S4a). This is promoted by severe twisting of aromatic rings in opposite directions with respect to each other (4ADB2 form I in Table 2). Form II has a needle- or rod-shaped morphology (4ADB2 in Figure S1) and it crystallizes in the monoclinic crystal system with the centrosymmetric space group $P2_1/c$ having one molecule in the asymmetric unit (Z' = 1, Figure 1l), where the molecules are primarily linked via bifurcated N1/C8−H1/H8···O1═C7 hydrogen bonds (red belts, Figure 4i). Here also the aromatic rings are severely twisted in the same direction with respect to the bridging amide and vinyl group (4ADB2 form II in Table 2), and this coplanarity in turn promotes alternate columns of $\pi\cdots\pi$ and C3−H3···F2A interactions (demarcated by blue and green belts, Figure 4i). Furthermore, the propagation of molecules along the c axis is facilitated by C12A−H12A···F2A/F1 and C13A−H13A···F1 interactions (Figure S4b). The crystal faces of both concomitant forms were experimentally indexed (form I, Figure 4a; form II, Figure 4c), and then the crystal habits were compared with their morphology prediction based on Bravais,[63] Friedel,[64] and Donnay and Harker[65] (BFDH) theory (Figure 4b,d). The BFDH method is a rapid method to identify the crystal morphology (hkl) that is most likely to form the crystal habit. The morphology and face indexation reveal that (100), (001), and (−101) are the major crystal faces of form I (Figure 4a), while (001) and (100) are the major crystal faces of form II (Figure 4c), which matches exactly with the predicted BFDH models.

2.3.2. Thermal and PXRD Analyses. The crystals of the two concomitant forms of 4ADB2 (optical image of the concomitant forms of 4ADB2 (form I + II) in Figure S1) were carefully separated by determinations of their unit cells using SCXRD experiments, and thereafter DSC experiments were performed in order to evaluate their individual thermal stabilities. The first and second heating−cooling cycles of form II (green and blue lines, respectively, in Figure 4g) show the presence of smooth endotherms with sharp melting peaks at 146 °C (ΔH = −99.0 J/g for the first cycle, ΔH = −101.0 J/g for the second cycle). On the other hand, the first heating−cooling cycle of form I (orange line in Figure 4g) displays a smooth endotherm with a single-crystal to single-crystal phase transition (SCSC-PT) occurring at 145 °C (ΔH = −22.6 J/g) immediately followed by its melting at 146 °C (ΔH = −111.0 J/g), which is the same as the melting point of form II, while in its second heating−cooling cycle (pink line in Figure 4g) the endotherm perfectly resembles that of form II, thereby indicating conversion of form I to the thermodynamically more stable form II. This indicates a complete structural transition from form I to form II at 145 °C and also suggests a greater thermal stability of form II over form I. An energy framework analysis shows that the dimers connected by N−H···O hydrogen bonds in form I have a much lower IE of −51.0 kJ/mol (form I in Figure 4j) in comparison to the dimers in form II linked via N−H···O hydrogen bonds with an IE of −58.2 kJ/mol (form II in Figure 4j). The molecular pairs linked via C−H···F interactions in form I have an IE of −12.8 kJ/mol (form I in Figure 4j), while the dimers in form II connected by a pair of C−H···F interactions related by an inversion center constitute a total IE of −23.1 kJ/mol (form II in Figure 4j), which implies that both forms have C−H···F interactions of almost similar strengths. Hence, energy frameworks clearly demonstrate the presence of stronger N−H···O hydrogen bonds in form II in comparison to form I, which makes the former more stable than the latter and hence also explains the irreversible SCSC-PT from the less stable polymorph form I to the thermodynamically more stable polymorph form II. The experimental PXRD patterns of the 4ADB2 bulk powder have been compared with the simulated PXRD patterns of both concomitant forms, and it has been found that the experimental pattern closely matches the simulated pattern of form I (Figure 4f), which has also been verified from a profile fitting refinement analysis, where only form I yielded satisfactory results after refinement (Figure S9c).

2.4. Polymorphs of 4ADB4: Forms I and II. *2.4.1. Molecular Packing.* 4ADB4 crystallizes in two polymorphic forms, both crystallizing in space group $P2_1/c$, having comparable unit cell parameters and one molecule in the asymmetric unit (Z' = 1, form I in Figure 1n, form II in Figure 1o) differing in their 3D packing arrangement. Interestingly, *in spite of considerable differences in the torsion angles of the molecules* (Table 2, 4ADB4 forms I and II) and crystal packing in the lattice, the packing differences are such that both polymorphic forms adopt the same unit cell parameters. Hence, this constitutes a prominent example of packing polymorphism. The crystal structure of form I illustrates that the molecules are primarily linked by N1−H1···O1═C7 hydrogen bonds, and this H-bonded arrangement is present in both modifications along the a axis in form I and along the b axis in form II (red bands in Figure 5d,e). However, Forms I and II differ in the way in which this

https://doi.org/10.1021/acs.cgd.1c00422
Cryst. Growth Des. 2021, 21, 4162−4177

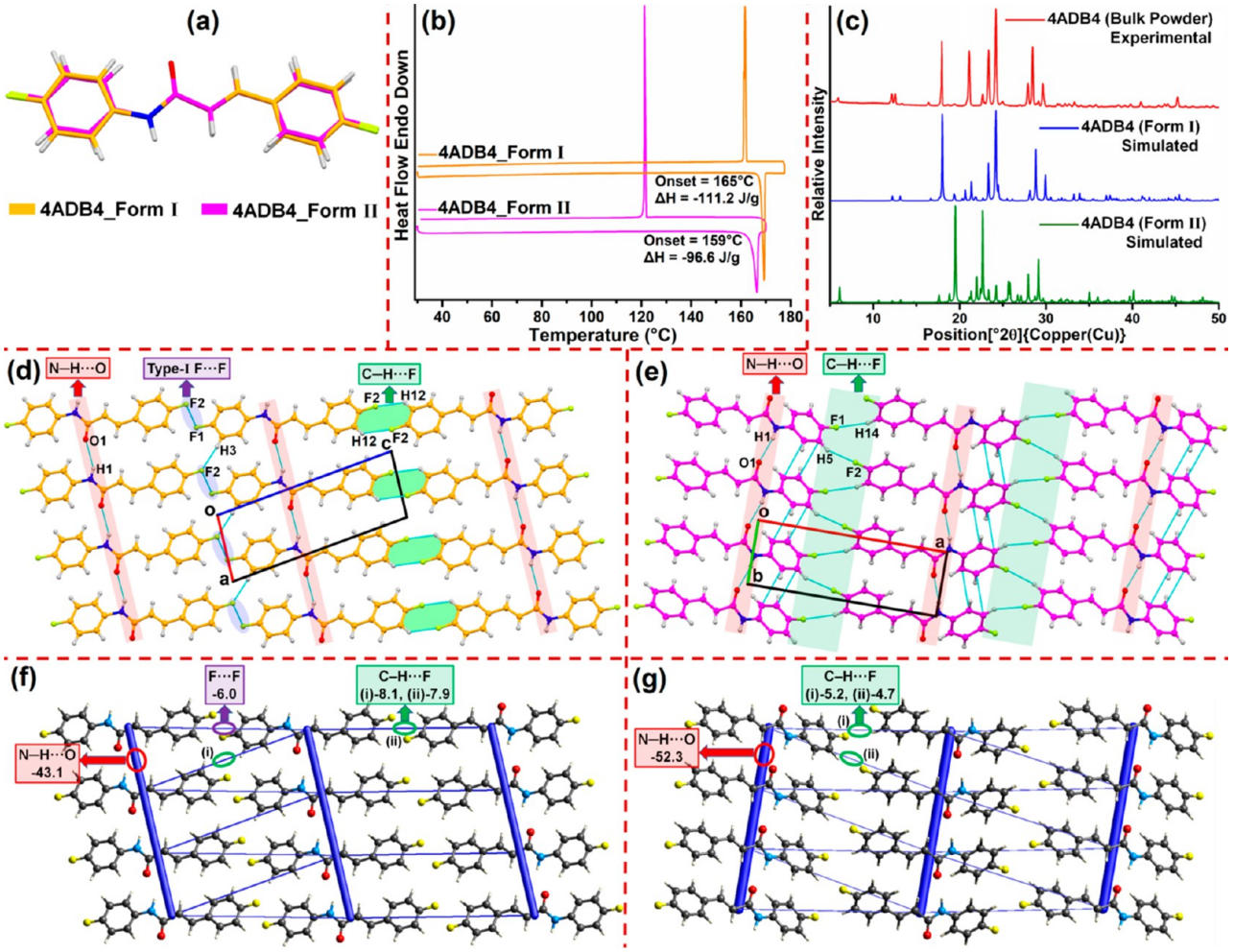

Figure 5. (a) Molecular overlay of two symmetry-independent molecules (one molecule each from form I and II of 4ADB4) at the solid-state geometry. (b) DSC profiles for the two forms of 4ADB4 at 3 °C/min of a heating−cooling cycle. (c) Overlay of PXRD patterns of 4ADB4 bulk powder and a comparison with the simulated patterns of their packing polymorphs. Crystal projections of (d) 4ADB4 (form I) and (e) 4ADB4 (form II) at 100 K. Energy frameworks for (f) form I and (g) form II of 4ADB4 representing the total interaction energies in kJ/mol.

common hydrogen bonded molecular chain is linked to its two neighboring units along their respective *c* and *a* axes. In form I the propagation of molecules along the *c* axis is favored by the formation of $R_2^2(8)$ C12−H12···F2 synthons (green zone in Figure 5d) and C3−H3···F2 interactions supported by C4−F1···F2−C13 Type-I ($\theta_1 = \theta_2 = 92°$) halogen−halogen contacts (purple ovals in Figure 5d), while in form II the translation of molecules along the *a* axis is promoted by C14−H14···F1 and C5−H5···F2 interactions (green belts in Figure 5e).

2.4.2. Thermal and PXRD Analyses. The two polymorphs were also examined by DSC, and the appearance of smooth baselines and sharp endothermic peaks suggests the presence of a single phase in the crystalline material (Figure 5b). The DSC curve of form I exhibits a melting peak at 165 °C ($\Delta H = -111.2$ J/g) (orange line in Figure 5b), whereas the melting point of form II is observed at 159 °C ($\Delta H = -96.6$ J/g) (magenta line in Figure 5b). Since form I melts at a much higher temperature and also exhibits a considerably higher enthalpy of fusion than form II, we can conclude from the "heat of fusion rule"[66] that the two polymorphs are monotropically related. A further confirmation that form I is the thermodynamically stable form over the entire temperature range can be derived from the order of their densities, i.e., form I > form II (Table S2), in accordance with the "density rule",[67,68] since the two forms differ mainly in the crystal packing of identical molecular units. An energy framework analysis shows that the N−H···O hydrogen-bonded dimers in form I have a much lower IE of −43.1 kJ/mol (red circle, Figure 5f) in comparison to form II, where the N−H···O hydrogen-bonded dimers are connected by a relatively higher IE of −52.3 kJ/mol (red circle, Figure 5g). This appears to be in stark contrast with the observations from DSC experiments, but the cumulative effect of weak C−H···F (IE = −8.1, −7.9 kJ/mol, Figure 5f) and type I F···F (IE = −6.0 kJ/mol, Figure 4f) interactions in form I in comparison to the much weaker C−H···F interactions in form II (IE = −5.2, −4.7 kJ/mol, Figure 5g) might be the reason behind the higher thermal stability of form I. This is a prime example of the important, cooperative, and supporting role of weak noncovalent interactions such as C−H···F and F···F alongside strong interactions such as N−H···O in steering the thermodynamic stability of molecular crystals. A comparison of the experimental powder pattern of the 4ADB4 bulk powder with the simulated powder patterns of the two packing polymorphs indicates that the bulk powder is representative of the more thermally stable form I (Figure 5c). This has also been verified from the satisfactory PXRD profile fitting refinement results obtained from only form I (Figure S9d).

https://doi.org/10.1021/acs.cgd.1c00422
Cryst. Growth Des. 2021, 21, 4162−4177

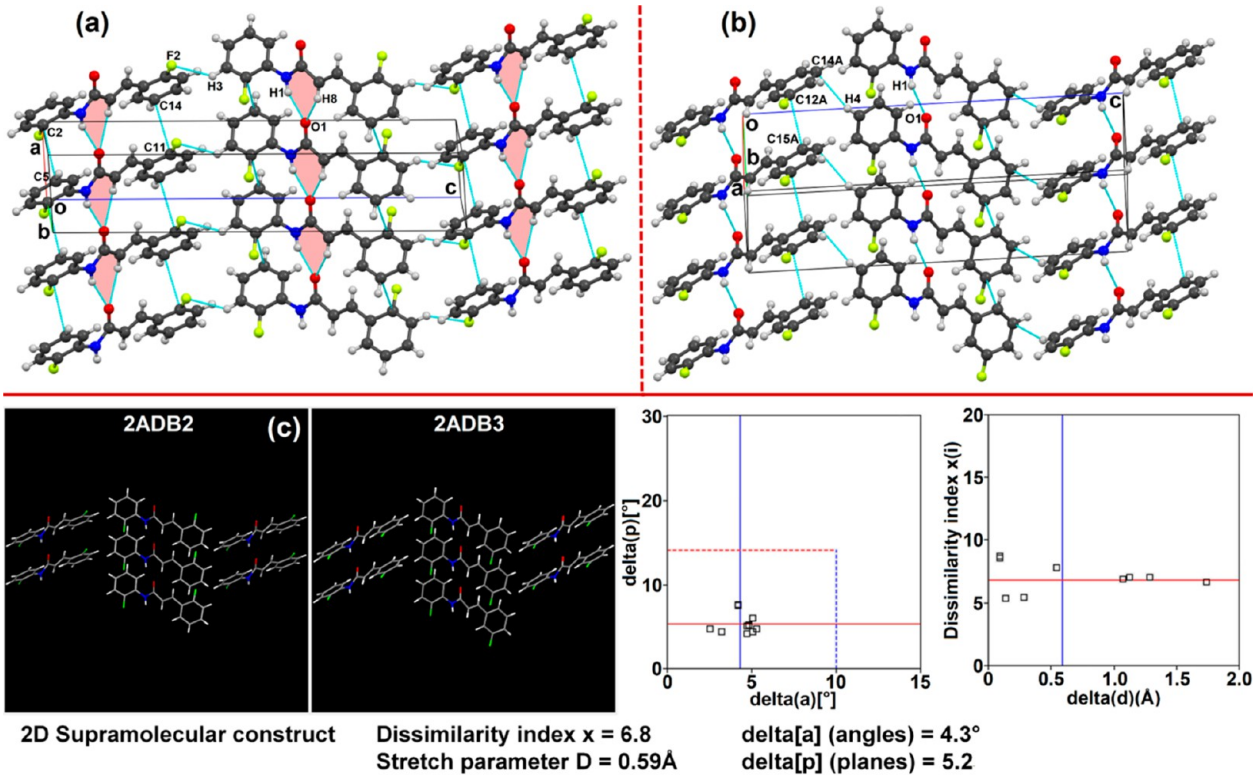

Figure 6. Molecular arrangements of (a) 2ADB2 and (b) 2ADB3, both along the *c* axis. (c) 2D supramolecular constructs obtained an from XPac analysis of 2ADB2−2ADB3.

2.5. Isostructural Analysis. To appreciate the role of intermolecular interactions in the design of similar molecular arrangements having equivalent structural motifs, we have quantitatively assessed the crystal packing similarities of unsubstituted *N*-phenylcinnamamide (ADB) with its difluoro-substituted analogues using XPac 2.0.2.[69−71] Two crystals having the same structure, i.e. similar molecular orientations and comparable arrangements in the lattice but not necessarily the same unit cell dimensions or chemical compositions, are said to exhibit isostructurality.[72−74] The structural similarities between two isostructural compounds can be expressed in terms of 1D molecular chains (a similar row of molecules), 2D molecular layers (a similar layer of molecules), or 3D supramolecular constructs (exactly similar arrangement or isostructural), while two crystals with the same space groups and identical unit cell dimensions are described as isomorphous.[75,76] It has been generally observed that isomorphous structures exhibit 3D isostructurality.[74] The extent to which two crystal structures deviate from perfect geometrical similarity is measured in terms of the "dissimilarity index (*X*)", where lower values of *X* are an indication of a better structural match. From our analysis it has been observed that some structures display 3D crystal packing similarity while others are related to each other via 2D packing similarity.

2.5.1. Comparison of 2ADB2 and 2ADB3. The single-crystal X-ray diffraction study reveals that both 2ADB2 and 2ADB3 crystallize in the monoclinic noncentrosymmetric space group *Pn* (*Z* = 2 for 2ADB2, *Z* = 4 for 2ADB3). Between these two structures, two crystallographic parameters (*a* and *c*) are similar, and the third (*b* axis) is just twice as large as the others (2ADB2) (Table S2). The orientation of one of the 2-fluoro-substituted benzene rings (C1 > C6) in 2ADB2 (rotation clockwise by 39.81(4)° from the vertical position) is opposite with respect to the orientation of the *o*-fluoro-substituted benzene ring (C1 > C6) in 2ADB3 (rotation anticlockwise by 34.35(6)° from the vertical position). Similarly, the orientation of the second *o*-fluoro-substituted benzene ring (C10 > C15) of 2ADB2 (rotation clockwise by 150.23(3)° or anticlockwise by 29.77° from the vertical position) is also opposite with respect to the orientation of the *p*-fluoro-substituted benzene ring (C10A > C15A) of 2ADB3 (rotation clockwise by 21.37(7)° from the vertical position). A crystal structure analysis of 2ADB2 shows that the molecules are primarily assembled via the formation of $R_2^1(6)$ N1/C8−H1/H8···O1═C7 hydrogen bond synthons supported by C2(π)···C5(π) and C11(π)···C14(π) interactions along the *a* axis having an IE of −55.9 kJ/mol, while their propagation along the *c* axis is promoted by C3−H3···F2 interactions with an IE of −7.5 kJ/mol (Figure 6a and Table S4). On the other hand, in the case of 2ADB3 the propagation of molecules along the *a* axis is facilitated by N1−H1···O1 hydrogen bonds supported by C12A(π)···C15A(π) interactions having an IE of −51.7 kJ/mol, while their spread along the *c* axis is promoted via C4−H4···C14A(π) interactions having an IE of −4.1 kJ/mol (Figure 6b and Table S4). Thus, a direct comparison of crystal packing patterns of 2ADB2−2ADB3 reveals similarity along the *a* and *c* crystallographic axes, and both virtually resemble the twisted-ribbon-like geometry. An XPac analysis of 2ADB2−2ADB3 reveals the presence of a 2D supramolecular construct (SC) with a dissimilarity index value of 6.8 (Figure 6c).

2.5.2. Comparison of 2ADB2 and 2ADB4 (Form II). The single-crystal X-ray data of 2ADB2 and 2ADB4 (form II) show that, despite having crystallized in the different noncentrosymmetric monoclinic space groups $P2_1$ and *Pn*, respectively, these two compounds have almost the same unit cell parameters (Table S2). A further comparison of their torsion angles also

https://doi.org/10.1021/acs.cgd.1c00422
Cryst. Growth Des. 2021, 21, 4162−4177

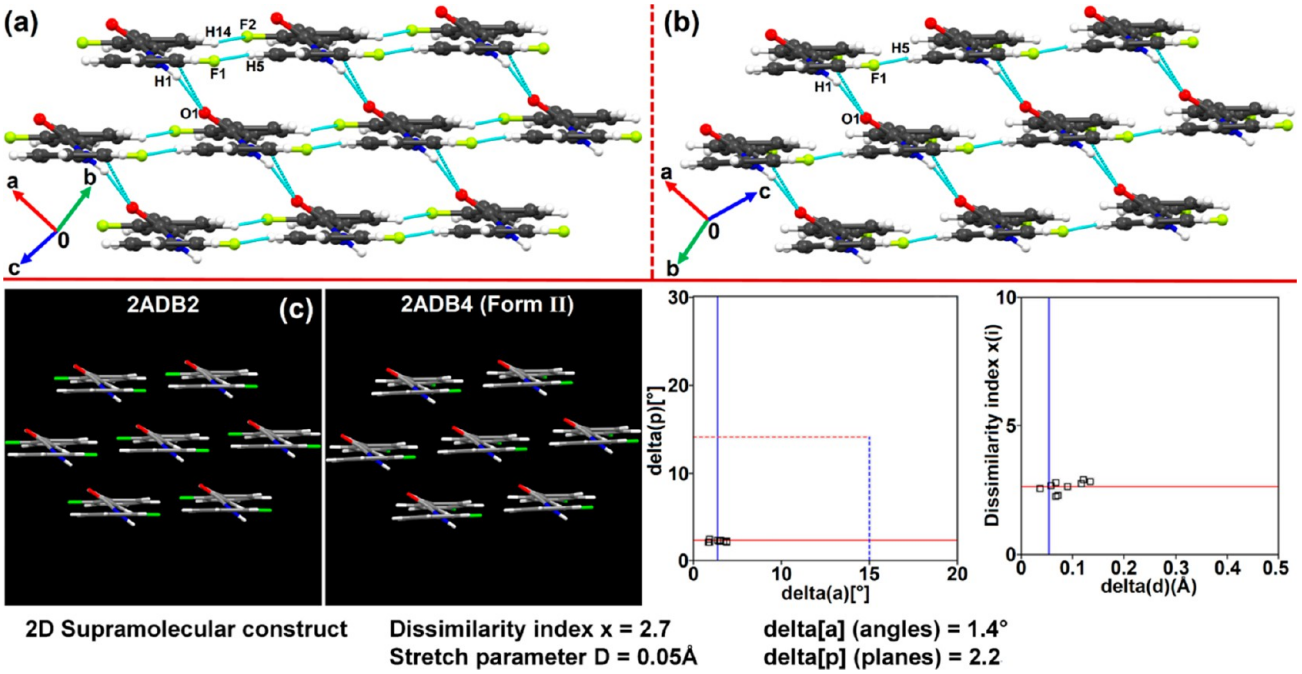

Figure 7. Molecular arrangements of (a) 2ADB2 and (b) 2ADB4 (form II). (c) 2D supramolecular constructs obtained from an XPac analysis of 2ADB2−2ADB4 (form II).

interestingly reveals that the orientation of one of the 2-fluoro-substituted benzene rings in 2ADB2 (C1 > C6) (rotation clockwise by 39.81(4)°) is the same as the orientation of the *o*-fluoro-substituted benzene ring in 2ADB4 (form II) (C1 > C6) (rotation clockwise by 39.13(3)°) (Table 1). Similarly, the orientation of the other 2-fluoro-substituted benzene ring in 2ADB2 (C10 > C15) (rotation clockwise by 150.22(3)°) is analogous to the orientation of the *p*-fluoro-substituted benzene ring in 2ADB4 (form II) (C10 > C15) (rotation clockwise by 152.26(3)°((Table 1). A crystal packing analysis of both compounds interestingly reveals that the molecules share exactly the same connectivity of $R_2^1(6)$ N1/C8−H1/H8···O1═C7 hydrogen bond synthons supported by C2(π)···C5(π) and C11(π)···C14(π) interactions along the *a* axis held by nearly equal IEs of −55.9 and −56.0 kJ/mol in 2ADB2 and 2ADB4 (form II), respectively (Figure 7a,b and Table S4). Furthermore, the molecules of both compounds are assembled in similar 1D molecular chains promoted via C5−H5···F1 and C14−H14···F2 interactions in 2ADB2 having an IE of −19.1 kJ/mol (Figure 7a and Table S4) and via C5−H5···F1 interactions and H12···H15 contacts in 2ADB4 (form II) having a similar IE of −19.9 kJ/mol (Figure 7b and Table S4). Therefore, a detailed comparison of the crystal packing of 2ADB2−2ADB4 (form II) reveals that these share closely related 2D-packing motifs, and an XPac analysis exhibits very close 2D crystal packing similarity with a very low dissimilarity index value of 2.7 (Figure 7c).

2.5.3. Comparison of 3ADB2 and 3ADB4. The crystal structures of 3ADB2 and 3ADB4 are isomorphous; both compounds have crystallized in the same space group *Pbca* and possess similar unit cell parameters with $Z = 8$ (Table S2). A crystal structure analysis of 3ADB2 shows that the molecules are primarily held via the formation of an $R_2^1(6)$ N1/C8−H1/H8···O1═C8 hydrogen bond synthon supported by $R_2^1(6)$ C14/C15−H14/H15···F1 synthons along the *b* axis having an IE of −54.9 kJ/mol, while C13−H13···F2 interactions connect them with an IE of −9.4 kJ/mol along the *a* axis (Figure S6a and Table S4). A top view of the structure of 3ADB2 along the *ac* plane reveals that the molecules are packed in a criss-cross fashion interlinked via C13−H13···F2 interactions down the *b* axis (Figure S6b). A structural analysis of 3ADB4 shows that propagation of molecules along the *b* axis is primarily facilitated by the formation of an $R_2^1(6)$ N1/C8−H1/H8···O1═C8 hydrogen bond synthon supported by $R_2^1(6)$ C11/C12−H11/H12···F1 interactions with an IE of −56.9 kJ/mol, while C12−H12···C14(π) interactions link them with an IE of −10.1 kJ/mol along the *a* axis (Figure S6c and Table S4). The crystal packing of 3ADB4 in a view along the *ac* plane reveals that the molecules have assembled in a criss-cross molecular architecture held together by C12−H12···C14(π) interactions (Figure S5d). Hence the overall crystal packing arrangements of 3ADB2 and 3ADB4 are also quite similar. An XPac analysis shows the presence of a 3D supramolecular construct with a dissimilarity index of 5.3 (Figure 8a).

2.5.4. Comparison of 3ADB3 (Form II) and 4ADB2 (Form I). Single-crystal data reveal that 3ADB3 (form II) and 4ADB2 (form I) have crystallized in the same monoclinic centrosymmetric space group *C*2/*c*, having very similar unit cell parameters with $Z = 8$ (Table S2). Hence the crystal structures 3ADB3 (form II)−4ADB2 (form I) can be classified as isomorphous. The orientation of one of the 3-fluorobenzene rings (C1 > C6) in 3ADB3 (form II) (rotation anticlockwise by −41.50(2)°) (Table 1) is similar to that of the 4-fluorobenzene ring (C1 > C6) in 4ADB2 (form I) (rotation anticlockwise by −41.38(13)°) (Table 2). Similarly, the orientation of the other 3-fluorobenzene ring (C10 > C15) in 3ADB3 (form II) (rotation clockwise by 161.79(6)°) (Table 1) is comparable to that of the 2-fluoro-substituted benzene ring (C10 > C15) in 4ADB2 (form I) (rotation clockwise by 160.39(13)°) (Table 2). Hence, a comparison of the torsion angles of these two polymorphs shows the presence of similar molecular conformations. A crystal structure analysis of both 3ADB3 (form II) and 4ADB2 (form I) shows that the molecules are primarily held

https://doi.org/10.1021/acs.cgd.1c00422
Cryst. Growth Des. 2021, 21, 4162−4177

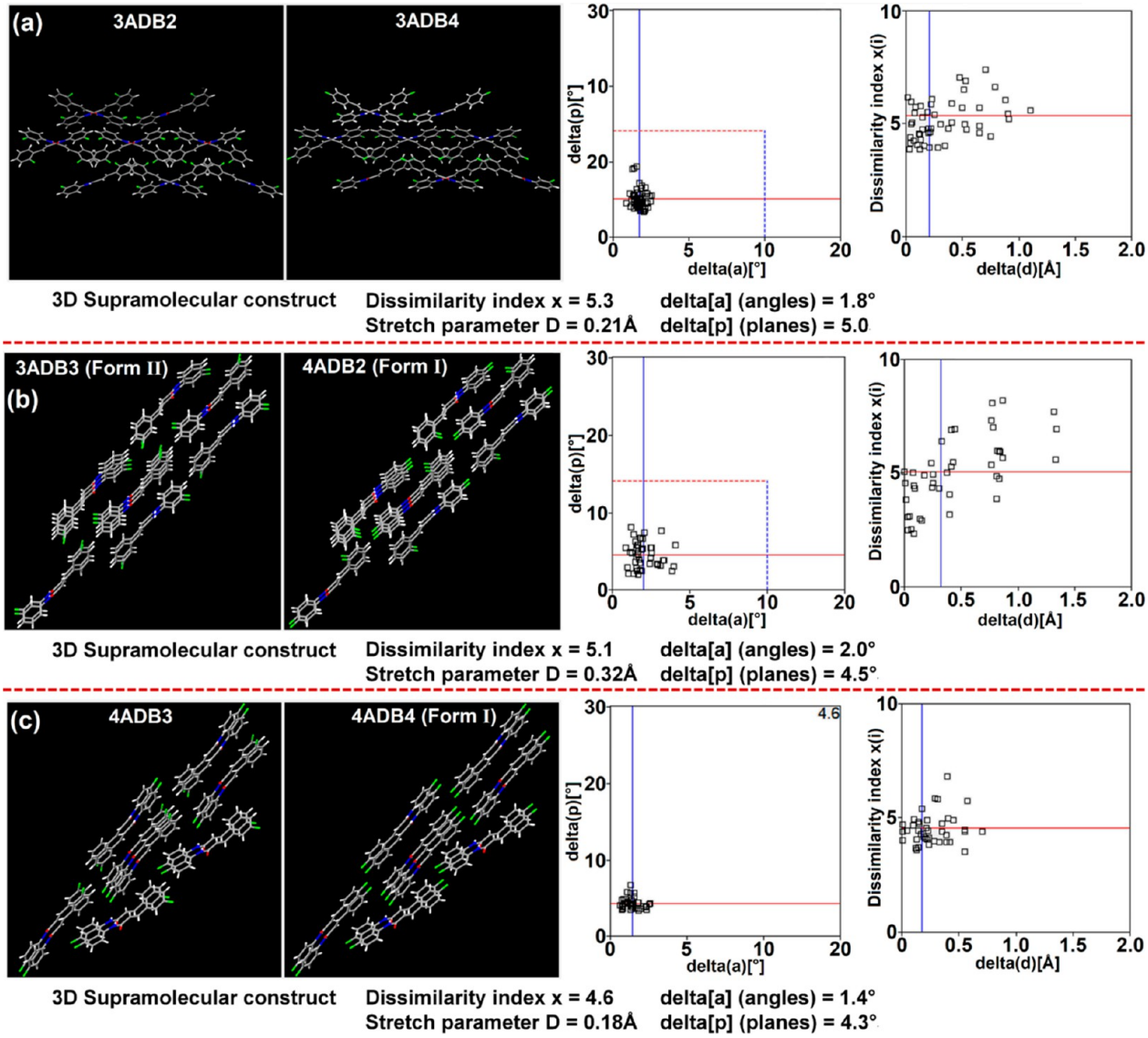

Figure 8. 3D supramolecular constructs obtained from an XPac analysis of (a) 3ADB2−3ADB4, (b) 3ADB3 (form II)−4ADB2 (form I), and (c) 4ADB3−4ADB4 (form I).

by N1−H1···O1 hydrogen bonds supported by $\pi\cdots\pi$ interactions along the *b* axis (Figures 3e and 4h) having comparable IEs of −54.5 and −51.0 kJ/mol, respectively (Table S4). The highly tilted orientation of the phenyl rings in both of the polymorphic forms facilitates alternate regions of C−H···F and C−H···π interactions along the *bc* plane (Figures S3b and S4a). In the case of 3ADB3 (form II), the molecules held by C−H···F interactions have an IE of −14.7 kJ/mol, while molecules held together by C−H···π interactions have IEs of −33.1 and −30.6 kJ/mol (Table S4). On the other hand, in the case of 4ADB2 (form I), molecules held by C−H···F interactions possess IEs of −6.0 and −12.8 kJ/mol, while dimers held by C−H···π interactions have IEs of −40.8 and −36.5 kJ/mol (Table S4). Thus, a detailed comparison of the crystal packing of 3ADB3 (form II) with that of 4ADB2 (form I) shows that the polymorphs share similar packing patterns along all three crystallographic axes. An XPac analysis reveals the presence of a 3D supramolecular construct with a dissimilarity index of 5.1 (Figure 8b).

2.5.5. Comparison of 4ADB3 and 4ADB4 (Form I). The single-crystal data of 4ADB3 and 4ADB4 (form I) show that both compounds have crystallized in the centrosymmetric monoclinic space group $P2_1/c$ with nearly the same unit cell parameters with $Z = 4$ (Table S2), suggesting that these two crystal structures are isomorphous. With respect to torsion angles, it was found that the orientation of one of the 4-fluoro-substituted benzene rings (C1 > C6) in 4ADB3 (rotation anticlockwise by −155.67(12)°) is similar to the orientation of the *p*-fluoro-substituted benzene ring (C1 > C6) in 4ADB4 (form I) (rotation anticlockwise by −161.59(12)°). Similarly, the orientation of the 3-fluoro-substituted benzene ring (C10 > C15) in 4ADB3 (rotation clockwise by 168.87(12)°) is also comparable with the orientation of the other *p*-fluoro-substituted benzene ring (C10 > C15) in 4ADB4 (form I) (rotation clockwise by 170.51(13)°) (Table 2). Hence, both compounds display similar molecular conformations. A comparison of their crystal structures reveals that molecules in both compounds are primarily held by N1−H1···O1 hydrogen bonds along the *a* axis having IEs of −46.5 and −43.1 kJ/mol in 4ADB3 and 4ADB4 (form I), respectively (Table S4). The propagation of molecules along the *c* axis is promoted via the

https://doi.org/10.1021/acs.cgd.1c00422
Cryst. Growth Des. 2021, 21, 4162−4177

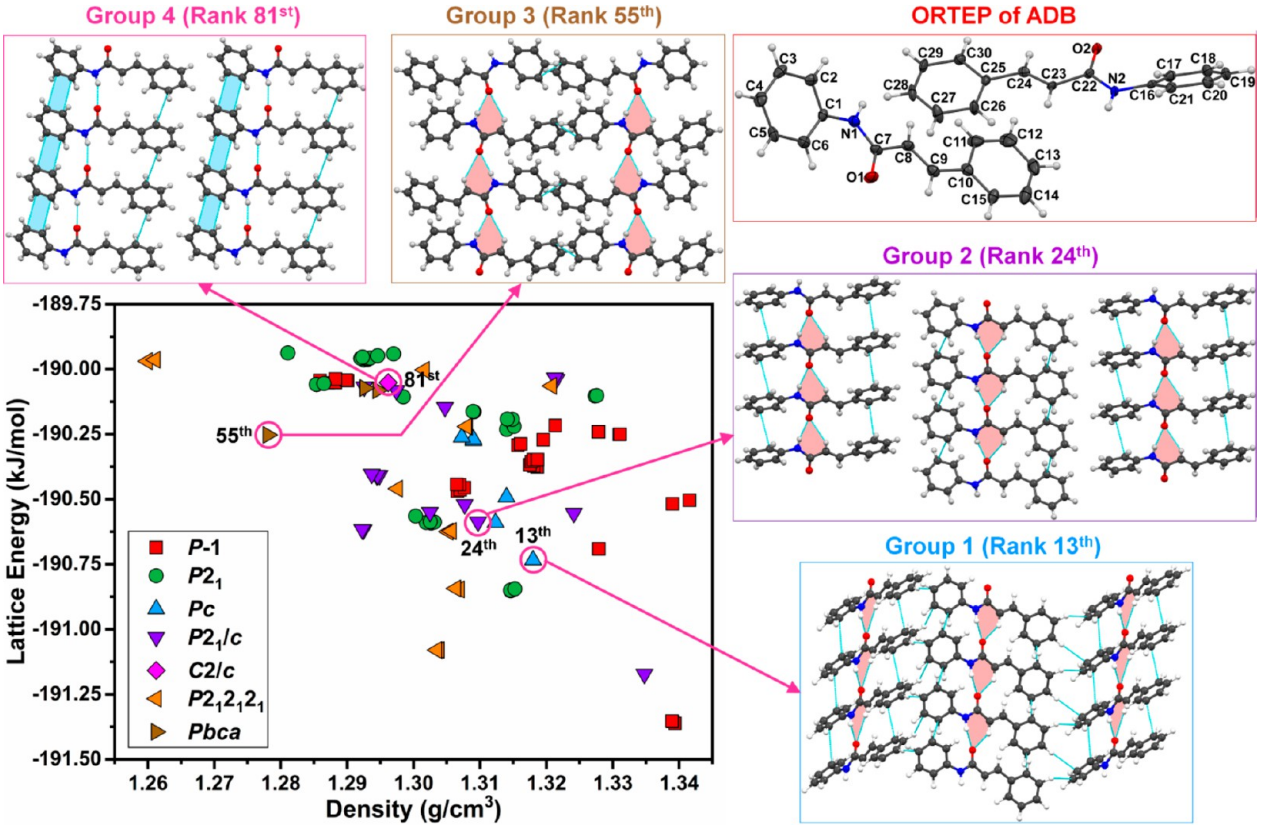

Figure 9. Lattice energy versus density plot for top 100 predicted structures on the basis of lattice energies, in various space groups of the parent unsubstituted compound ADB, with the identification of predicted structures analogous to the experimentally obtained crystal structures along their lowest energy rank.

Table 3. Classification of Experimental Crystal Structures of Difluoro-Substituted ADB Molecules within the Top 100 Predicted Structures in the CSP Landscape of ADB

		unit cell type			space group	
group	rank	predicted	exptl	compound	exptl	predicted
group 1	13th	24−5−23	5−5−24	2ADB2	*Pn*	*Pc*
			5−11−22	2ADB3	*Pn*	
			5−5−23	2ADB4 (form II)	$P2_1$	
group 2	24th	10−5−25	10−5−24	4ADB2 (form II)	$P2_1/c$	$P2_1/c$
group 3	55th	11−9−22	12−10−22	3ADB2	*Pbca*	*Pbca*
			10−10−26	3ADB3 (form III)	$P2_12_12_1$	
			12−9−21	3ADB4	*Pbca*	
group 4	81st	30−5−16	30−5−16	3ADB3 (form II)	*C*2/*c*	*C*2/*c*
			30−5−16	4ADB2 (form I)	*C*2/*c*	

formation of similar $R_2^2(8)$ C13−H13···F2 interactions in 4ADB3 (IE = 9.1 kJ/mol) and $R_2^2(8)$ C12−H12···F2 interactions in 4ADB4 (form I) (IE = −7.9 kJ/mol) on one end of the molecule and via the formation of F1(lp)···C13(π) interactions in 4ADB3 (IE = −5.6 kJ/mol) and a type I F1···F2 halogen−halogen contact in 4ADB4 (form I) (IE = −6.0 kJ/mol) on the other end leading to the formation of almost identical 1-D molecular chains (Figure 5d and Figure S7a). The view along the *bc* plane reveals that molecules have assembled in a double-herringbone fashion with the molecular dimers related by inversion centers along the *c* axis. These dimers are connected via C11−H11···O1 hydrogen bonds supported by C3−H3···F2 interactions in 4ADB3 (IE = −34.5 kJ/mol) (Figure S5a), while those in 4ADB4 (form I) are connected via only C11−H11···O1 hydrogen bonds (IE = −26.5 kJ/mol) (Figure S7b). Therefore, a detailed comparison of the crystal packing patterns of 4ADB3 with 4ADB4 (form I) reflects their isostructural behavior. An XPac analysis further reveals the presence of a 3D supramolecular construct with a dissimilarity index of 4.6 (Figure 8c).

2.6. Crystal Structure Prediction (CSP). In this study, the occurrence of different packing motifs in the crystal structures of synthesized difluoro-substituted ADB molecules was examined by generating the crystal structure landscape (CSL) of the unsubstituted ADB molecule (see the ORTEP drawing of ADB in Figure 9). The CSL of the given compound has been generated on account of the variations in molecular conformation and molecular self-assembly for different packing motifs during the crystallization process. For this purpose, the crystal geometry of ADB was optimized by the dispersion correction method in conjunction with assignment of electro-

https://doi.org/10.1021/acs.cgd.1c00422
Cryst. Growth Des. 2021, 21, 4162−4177

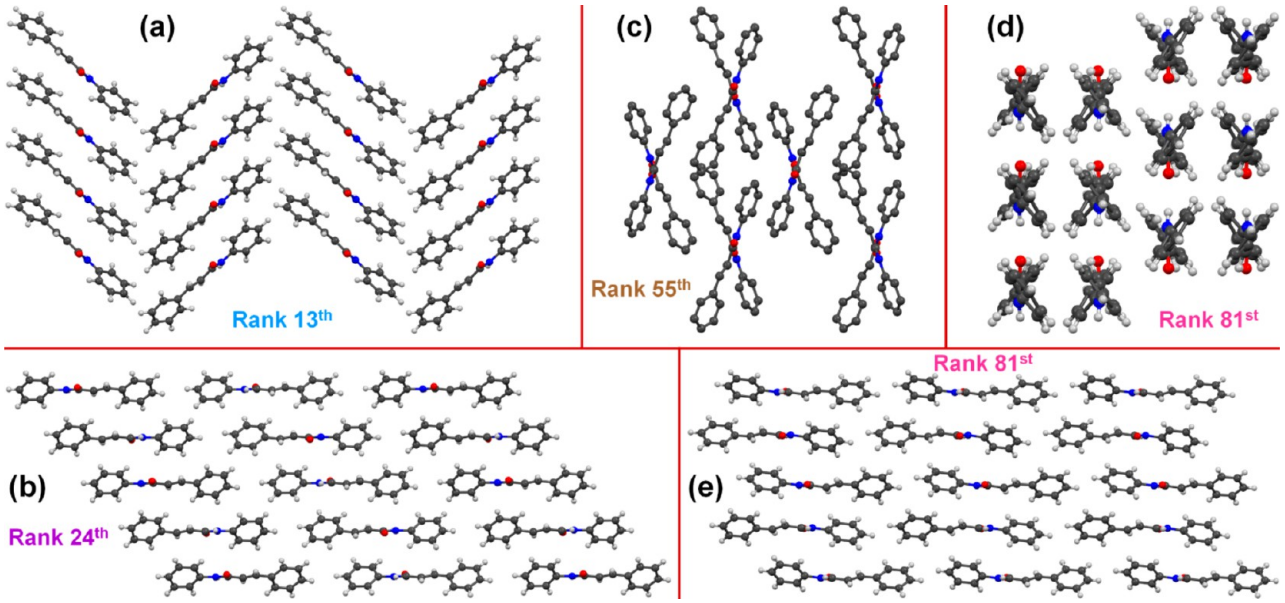

Figure 10. Supramolecular predicted structures of ADB bearing resemblance with the experimentally obtained crystal structures of difluoro-substituted ADB molecules with their lowest energy ranks: (a) rank 13, (b) rank 24, (c) rank 55, (d, e) rank 81.

static surface potential (ESP) charges on all the atoms, which serves as the starting point for structure prediction. The calculations were performed using the DMol3 module followed by Polymorph Prediction utilizing the COMPASS27 force field incorporated in the Materials Studio 6.1 program package. We have chosen the default setup entitled "Fine Quality" for packing, geometry optimization, and clustering. The calculation for structure prediction was limited to 7 experimentally observed space groups ($P\bar{1}$, $P2_1$, Pc, $P2_1/c$, $C2/c$, $P2_12_12_1$, and $Pbca$), while only the top 100 energy-minimized predicted structures were chosen among more than 5000 generated structures for analysis with respect to high density, as shown in the lattice energy vs crystal density plot in Figure 9.

In our current CSP analysis, the analysis of the crystal landscape has been carried out by classifying the experimentally obtained crystal structures of difluoro-substituted ADB molecules into groups on the basis of preferences of their molecular orientations, packing motifs, and global interaction topologies, irrespective of their unit cell parameters (Table 3). The CSP results show that the 13th rank (−190.7 kJ/mol) among the predicted structures with space group *Pc* has a molecular packing pattern very similar to the experimentally obtained crystal structures of 2ADB2, 2ADB3, and 2ADB4 (form II), which have been collectively labeled as Group 1. The molecules in the predicted structure are assembled in a twisted-ribbon-like architecture held by $R_2^1(6)$ N/C−H···O═C hydrogen bond synthons (see group 1, rank 13th in Figure 9), which bears close resemblance to the twisted-ribbon-like self-assembly of 2ADB2 (Figure 6a), 2ADB3 (Figure 6b), and 2ADB4 (form II) (Figure S2b). The predicted structure in a view down the N/C−H···O═C hydrogen bonds displays a wavelike herringbone architecture (Figure 10a), which also closely matches the herringbone crystal packing in 2ADB2 (Figure S10a), 2ADB3 (Figure S10b), and 2ADB4 (form II) (Figure S10c). The 24th rank in the predicted structure with space group $P2_1/c$ has a linear twisted-ribbon-like molecular packing arrangement held by $R_2^1(6)$ N/C−H/H···O═C hydrogen bond synthons (see group 2, rank 24th in Figure 9), which is similar to the experimentally determined crystal packing motif of 4ADB2 (form II). The predicted structure in a view down the N/C−H···O═C hydrogen bonds displays a parallel-displaced layered molecular stacking arrangement (Figure 10b) very similar to the layered assembly of molecules in the crystal packing of 4ADB2 (form II) (Figure S10d). The experimentally obtained crystal systems having orthorhombic space groups, namely 3ADB2, 3ADB3 (form III), and 3ADB4, have been collectively labeled as group 3 and are ranked 55th in the CSL landscape of ADB (see group 3, rank 55 in Figure 9). The molecules in this predicted structure are primarily held by $R_2^1(6)$ N/C−H···O═C hydrogen bond synthons. A top view down these N−H···O═C hydrogen-bonded chains reveals a unique criss-cross molecular assembly (Figure 10c) that is perfectly commensurate with the criss-cross molecular architectures of 3ADB2 (Figure S6b), 3ADB3 (form III), and 3ADB4 (Figure S6d). The experimentally obtained crystal systems with monoclinic space group $C2/c$, namely 3ADB3 (form II) and 4ADB2 (form I), have been labeled as group 4 and have been ranked 81st in the energy landscape. The molecules in this predicted structure are held via N−H···O hydrogen bonds supported by $\pi\cdots\pi$ interactions (see group 4, rank 81 in Figure 9), and this pattern manifests itself in the crystal packing of 3ADB3 (form II) (Figure S10e) and 4ADB2 (form I) (Figure S10f). The two benzene rings of ADB in this rank are oppositely oriented and have assembled in a columnar fashion via N−H···O hydrogen bonds (Figure 10d), which closely corresponds with the columnar assembly in 3ADB3 (form II) (Figure 3e) and 4ADB2 (form I) (Figure 4h). Moreover, the crystal structure of ADB in this rank displays a brick-layered packing (Figure 10e) in a view from above the N−H···O hydrogen bond columns; this pattern bears close resemblance with the brick-layered molecular assembly in 3ADB3 (form II) (Figure S3b) and 4ADB2 (form I) (Figure S4a). Hence, we have been able to identify the occurrence of only 9 out of a total of 15 experimentally obtained difluoro-substituted ADB crystals in the low-energy ranks of the computed energy landscape (see Table 3) with the complete absence of the remaining 6 unit cells in the predicted structures. Interestingly it has been observed that the crystal structure

https://doi.org/10.1021/acs.cgd.1c00422
Cryst. Growth Des. 2021, 21, 4162−4177

similar to 4ADB2 (form II) (24th rank) is more stable than the structure similar to 4ADB2 (form I) (81st rank), which perfectly concurs with our experimental findings, where it was observed that 4ADB2 (form I) experiences a SCSC phase transition to its more stable form 4ADB2 (form II) (see Figure 4g). 3ADB3 (form I) is a solvatomorph, and hence its crystal-packing motif is absent from this computed landscape, but the crystal packing arrangements of the other two polymorphs 3ADB3 (form II) (81st rank) and 3ADB3 (form III) (55th rank) were identified in the landscape. The order of their lattice energies perfectly coincides with the thermal stabilities of both forms, where it was observed that 3ADB3 (form II) displayed a much lower melting point (117 °C) in comparison to 3ADB3 (form III) (127 °C) (see Figure 3b). These results suggest that, although a few packing motifs could not be identified in the top 100 predicted structures, CSP nevertheless has been able to correctly predict the order of stabilities of the few polymorphs whose structures were identified in the energy landscape.

3. SUMMARY

In conclusion, the role of weak intermolecular interactions in a family of unsubstituted and difluoro-substituted *N*-phenyl-cinnamamides (ADB) (total of 10 molecules, See Scheme 1) has been quantitatively analyzed by simply changing the position of the fluorine atoms from *ortho* to *meta* to *para* in different isomeric molecules and via isolation of their different polymorphic forms by employing an extensive crystallization strategy. Interestingly, four difluorinated derivatives of ADB have been found to exhibit polymorphic behavior with distinct thermal properties. The structural and energetic origins of molecular associations in this class of molecules have been investigated in detail, and it has been found that this unique structural fragment is highly polymorphic in nature and hence can be termed as a polymorphophore. The crystal structures of these molecules have been analyzed in terms of their molecular packing motifs, which exhibit isomorphism and isostructurality in the solid state. The molecules have been found to exploit the most energetically favored intermolecular N−H···O═C chain hydrogen bond synthons to build their supramolecular assemblies, each in a different fashion to accommodate the weaker secondary C−H···F, C−H···π, π···π, and in one case type II C−F···F−C contacts. The cooperative interplay among these various intermolecular interactions (strong and weak) and the flexibilities associated with them are instrumental in the local variations of different structural types, which enhances the possibilities of their polymorphic outcomes. CSP calculations have been performed on the solid-state structure of the highly flexible unsubstituted ADB molecule, aiming to explore the large number of possible structures for its difluorinated derivatives, among which the experimental polymorphs were likely to be found. Herein, the top 100 predicted structures on the basis of their lattice energies were selected for a direct comparison of their packing motifs with the experimentally realized crystal structures. The results from CSP analysis demonstrate the successful prediction of most of the experimental structures in the computed energy landscape, which also represents an advancement in CSP methodology.

■ ASSOCIATED CONTENT

Supporting Information

The Supporting Information is available free of charge at https://pubs.acs.org/doi/10.1021/acs.cgd.1c00422.

Experimental details, including details of crystallization screening, images of crystal morphologies, description of SCXRD data collection and structure refinements, additional images of molecular packing, DSC traces, refinement of PXRD patterns, details of interaction energy frameworks, and results from CSP calculations (PDF)

Accession Codes

CCDC 1834349−1834358, 2075169, 2075171, 2075173, and 2075175−2075177 contain the supplementary crystallographic data for this paper. These data can be obtained free of charge via www.ccdc.cam.ac.uk/data_request/cif, or by emailing data_request@ccdc.cam.ac.uk, or by contacting The Cambridge Crystallographic Data Centre, 12 Union Road, Cambridge CB2 1EZ, UK; fax: +44 1223 336033.

■ AUTHOR INFORMATION

Corresponding Authors

Rohit Bhowal − *Crystallography and Crystal Chemistry Laboratory, Department of Chemistry, Indian Institute of Science Education and Research Bhopal, Bhopal 462066, Madhya Pradesh, India*; Email: rohitbh@iiserb.ac.in

Deepak Chopra − *Crystallography and Crystal Chemistry Laboratory, Department of Chemistry, Indian Institute of Science Education and Research Bhopal, Bhopal 462066, Madhya Pradesh, India*; orcid.org/0000-0002-0018-6007; Email: dchopra@iiserb.ac.in

Complete contact information is available at: https://pubs.acs.org/10.1021/acs.cgd.1c00422

Notes

The authors declare no competing financial interest.

■ ACKNOWLEDGMENTS

R.B. acknowledges IISERB for research fellowship. We thank IISER Bhopal for research facilities and infrastructure.

■ REFERENCES

(1) Gouverneur, V.; Seppelt, K. Introduction: Fluorine Chemistry. *Chem. Rev.* **2015**, *115*, 563−565.

(2) Ojima, I. Exploration of Fluorine Chemistry at the Multidisciplinary Interface of Chemistry and Biology. *J. Org. Chem.* **2013**, *78*, 6358−6383.

(3) Berger, R.; Resnati, G.; Metrangolo, P.; Weberd, E.; Hulliger, J. Organic fluorine compounds: a great opportunity for enhanced materials properties. *Chem. Soc. Rev.* **2011**, *40*, 3496−3508.

(4) Meanwell, N. A. Fluorine and Fluorinated Motifs in the Design and Application of Bioisosteres for Drug Design. *J. Med. Chem.* **2018**, *61*, 5822−5880.

(5) Gillis, E. P.; Eastman, K. J.; Hill, M. D.; Donnelly, D. J.; Meanwell, N. A. Applications of Fluorine in Medicinal Chemistry. *J. Med. Chem.* **2015**, *58*, 8315−8359.

(6) Harsanyi, A.; Sandford, G. Organofluorine chemistry: applications, sources and sustainability. *Green Chem.* **2015**, *17*, 2081−2086.

(7) Xing, L.; Blakemore, D. C.; Narayanan, A.; Unwalla, R.; Lovering, F.; Denny, R. A.; Zhou, H.; Bunnage, M. E. Fluorine in Drug Design: A Case Study with Fluoroanisoles. *ChemMedChem* **2015**, *10*, 715−726.

(8) Han, J.; Remete, A. M.; Dobson, L. S.; Kiss, L.; Izawa, K.; Moriwaki, H.; Soloshonok, V. A.; O'Hagan, D. Next generation organofluorine containing blockbuster drugs. *J. Fluorine Chem.* **2020**, *239*, 109639.

(9) Mei, H.; Han, J.; Fustero, S.; Medio-Simon, M.; Sedgwick, D. M.; Santi, C.; Ruzziconi, R.; Soloshonok, V. A. Fluorine-Containing Drugs Approved by the FDA in 2018. *Chem. - Eur. J.* **2019**, *25*, 11797−11819.

(10) O'Hagan, D. Fluorine in health care: Organofluorine containing blockbuster drugs. *J. Fluorine Chem.* **2010**, *131*, 1071−1081.
(11) Wang, J.; Sánchez-Roselló, M.; Aceña, J. L.; del Pozo, C.; Sorochinsky, A. E.; Fustero, S.; Soloshonok, V. A.; Liu, H. Fluorine in Pharmaceutical Industry: Fluorine-Containing Drugs Introduced to the Market in the Last Decade (2001−2011). *Chem. Rev.* **2014**, *114*, 2432−2506.
(12) Inoue, M.; Sumii, Y.; Shibata, N. Contribution of Organofluorine Compounds to Pharmaceuticals. *ACS Omega* **2020**, *5*, 10633−10640.
(13) Yoder, N. C.; Kumar, K. Fluorinated amino acids in protein design and engineering. *Chem. Soc. Rev.* **2002**, *31*, 335−341.
(14) Berger, A. A.; Völler, J. S.; Budisa, N.; Koksch, B. Deciphering the Fluorine Code−The Many Hats Fluorine Wears in a Protein Environment. *Acc. Chem. Res.* **2017**, *50*, 2093−2103.
(15) Mei, H.; Han, J.; Klika, K. D.; Izawa, K.; Sato, T.; Meanwell, N. A.; Soloshonok, V. A. Applications of fluorine-containing amino acids for drug design. *Eur. J. Med. Chem.* **2020**, *186*, 111826.
(16) Cimarosti, Z.; Castagnoli, C.; Rossetti, M.; Scarati, M.; Day, C.; Johnson, B.; Westerduin, P. Development of Drug Substances as Mixture of Polymorphs: Studies to Control Form 3 in Casopitant Mesylate. *Org. Process Res. Dev.* **2010**, *14*, 1337−1346.
(17) Marques, M. P. M.; Valero, R.; Parker, S. F.; Tomkinson, J.; Batista de Carvalho, L. A. E. Polymorphism in Cisplatin Anticancer Drug. *J. Phys. Chem. B* **2013**, *117*, 6421−6429.
(18) Park, Y.; Boerrigter, S. X. M.; Yeon, J.; Lee, S. H.; Kang, S. K.; Lee, E. H. New Metastable Packing Polymorph of Donepezil Grown on Stable Polymorph Substrates. *Cryst. Growth Des.* **2016**, *16*, 2552−2560.
(19) Blandizzi, C.; Viscomi, G. C.; Scarpignato, C. Impact of crystal polymorphism on the systemic bioavailability of rifaximin, an antibiotic acting locally in the gastrointestinal tract, in healthy volunteers. *Drug Des., Dev. Ther.* **2014**, *9*, 1−11.
(20) Chemburkar, S. R.; Bauer, J.; Deming, K.; Spiwek, H.; Patel, K.; Morris, J.; Henry, R.; Spanton, S.; Dziki, W.; Porter, W.; Quick, J.; Bauer, P.; Donaubauer, J.; Narayanan, B. A.; Soldani, M.; Riley, D.; McFarland, K. Dealing with the Impact of Ritonavir Polymorphs on the Late Stages of Bulk Drug Process Development. *Org. Process Res. Dev.* **2000**, *4*, 413−417.
(21) Terada, S.; Katagiri, K.; Masu, H.; Danjo, H.; Sei, Y.; Kawahata, M.; Tominaga, M.; Yamaguchi, K.; Azumaya, I. Polymorphism of Aromatic Sulfonamides with Fluorine Groups. *Cryst. Growth Des.* **2012**, *12*, 2908−2916.
(22) Cruz-Cabeza, A. J.; Reutzel-Edensb, S. M.; Bernstein, J. Facts and fictions about polymorphism. *Chem. Soc. Rev.* **2015**, *44*, 8619−8635.
(23) Gentili, D.; Gazzano, M.; Melucci, M.; Jones, D.; Cavallini, M. Polymorphism as an additional functionality of materials for technological applications at surfaces and interfaces. *Chem. Soc. Rev.* **2019**, *48*, 2502−2517.
(24) Cruz-Cabeza, A. J.; Bernstein, J. Conformational Polymorphism. *Chem. Rev.* **2014**, *114*, 2170−2191.
(25) McCrone, W. C. Polymorphism. In *Physics and Chemistry of the Organic Solid State*; Fox, D., Labes, M. M., Weissberger, A., Eds.; Wiley Interscience: New York, 1965; Vol. 2, pp 725−767.
(26) Nangia, A.; Desiraju, G. R. Pseudopolymorphism: occurrences of hydrogen bonding organic solvents in molecular crystals. *Chem. Commun.* **1999**, 605−606.
(27) Chopra, D.; Guru Row, T. N. Solvatomorphism in 3-Fluorobenzoylaminophenyl 3-Fluorobenzoate: A Subtle Interplay of Strong Hydrogen Bonds and Weak Intermolecular Interactions Involving Disordered Fluorine. *Cryst. Growth Des.* **2006**, *6* (6), 1267−1270.
(28) Dey, D.; Chopra, D. Solvatomorphism in (Z)-4-fluoro-N′-(3-fluorophenyl)benzimidamide: the role of intermolecular O−H···F interaction. *CrystEngComm* **2016**, *18*, 8291−8300.
(29) Bernstein, J.; Davey, R. J.; Henck, J. O. Concomitant Polymorphs. *Angew. Chem., Int. Ed.* **1999**, *38*, 3440−3461.
(30) Ruggiero, M. T.; Zeitler, J. A.; Korter, T. M. Concomitant polymorphism and the martensitic-like transformation of an organic crystal. *Phys. Chem. Chem. Phys.* **2017**, *19*, 28502−28506.
(31) Tang, W.; Sima, A. D.; Gong, J.; Wang, J.; Li, T. Kinetic Difference between Concomitant Polymorphism and Solvent-Mediated Phase Transformation: A Case of Tolfenamic Acid. *Cryst. Growth Des.* **2020**, *20*, 1779−1788.
(32) Park, Y.; Boerrigter, S. X. M.; Yeon, J.; Lee, S. H.; Kang, S. K.; Lee, E. H. New Metastable Packing Polymorph of Donepezil Grown on Stable Polymorph Substrates. *Cryst. Growth Des.* **2016**, *16*, 2552−2560.
(33) Kasuga, N. C.; Saito, Y.; Satob, H.; Yamaguchi, K. Packing polymorphism in the crystal structure of 4,5-dimethoxy-2-nitrobenzyl acetate. *Acta Crystallogr.* **2015**, *71*, 483−486.
(34) Purdum, G. E.; Telesz, N. G.; Jarolimek, K.; Ryno, S. M.; Gessner, T.; Davy, N. C.; Petty, A. J.; Zhen, Y.; Shu, Y.; Facchetti, A.; Collis, G. E.; Hu, W.; Wu, C.; Anthony, J. E.; Weitz, R. T.; Risko, C.; Loo, Y.-L. Presence of Short Intermolecular Contacts Screens for Kinetic Stability in Packing Polymorphs. *J. Am. Chem. Soc.* **2018**, *140*, 7519−7525.
(35) Rai, S. K.; Gunnam, A.; Mannava, M. K. C.; Nangia, A. K. Improving the Dissolution Rate of the Anticancer Drug Dabrafenib. *Cryst. Growth Des.* **2020**, *20*, 1035−1046.
(36) Skieneh, J. M.; Sathisaran, I.; Dalvi, S. V.; Rohani, S. Co-amorphous Form of Curcumin−Folic Acid Dihydrate with Increased Dissolution Rate. *Cryst. Growth Des.* **2017**, *17*, 6273−6280.
(37) Nicoud, L.; Licordari, F.; Myerson, A. S. Estimation of the Solubility of Metastable Polymorphs: A Critical Review. *Cryst. Growth Des.* **2018**, *18*, 7228−7237.
(38) Hu, S.; Mishra, M. K.; Sun, C. C. Twistable Pharmaceutical Crystal Exhibiting Exceptional Plasticity and Tabletability. *Chem. Mater.* **2019**, *31*, 3818−3822.
(39) Chen, H.; Wang, C.; Sun, C. C. Profoundly Improved Plasticity and Tabletability of Griseofulvin by in Situ Solvation and Desolvation during Spherical Crystallization. *Cryst. Growth Des.* **2019**, *19*, 2350−2357.
(40) Liu, G.; Xiong, Y.; Gou, R.; Zhang, C. Difference in the Thermal Stability of Polymorphic Organic Crystals: A Comparative Study of the Early Events of the Thermal Decay of 2,4,6,8,10,12-Hexanitro-2,4,6,8,10,12-hexaazaisowurtzitane (CL-20) Polymorphs under the Volume Constraint Condition. *J. Phys. Chem. C* **2019**, *123*, 16565−16576.
(41) Nokhodchi, A.; Homayouni, A.; Araya, R.; Kaialy, W.; Obeidat, W.; Asare-Addo, K. Crystal engineering of ibuprofen using starch derivatives in crystallization medium to produce promising ibuprofen with improved pharmaceutical performance. *RSC Adv.* **2015**, *5*, 46119−46131.
(42) Diniz, L. F.; Carvalho, P. S., Jr.; de Melo, C. C.; Ellena, J. Reducing the Hygroscopicity of the Anti-Tuberculosis Drug (S,S)-Ethambutol Using Multicomponent Crystal Forms. *Cryst. Growth Des.* **2017**, *17*, 2622−2630.
(43) Thakur, T. S.; Thakuria, R. Crystalline Multicomponent Solids: An Alternative for Addressing the Hygroscopicity Issue in Pharmaceutical Materials. *Cryst. Growth Des.* **2020**, *20*, 6245−6265.
(44) Nelson, M. R.; Johnson, T.; Warren, L.; Hughes, A. R.; Chissoe, S. L.; Xu, C.-F.; Waterworth, D. M. The genetics of drug efficacy: opportunities and challenges. *Nat. Rev. Genet.* **2016**, *17*, 197−206.
(45) Suresh, K.; Nangia, A. Curcumin: pharmaceutical solids as a platform to improve solubility and bioavailability. *CrystEngComm* **2018**, *20*, 3277−3296.
(46) Vo, A. H.; Van Vleet, T. R.; Gupta, R. R.; Liguori, M. J.; Rao, M. S. An Overview of Machine Learning and Big Data for Drug Toxicity Evaluation. *Chem. Res. Toxicol.* **2020**, *33*, 20−37.
(47) Dixit, V. A. A simple model to solve a complex drug toxicity problem. *Toxicol. Res.* **2019**, *8*, 157−171.
(48) von Liebig, J.; Wöhler, F. Unter suchengen über das Radikal der Benzosäure. *Ann. Pharm.* **1832**, *3*, 249−282.
(49) Panini, P.; Chopra, D. Experimental and Theoretical Characterization of Short H-Bonds with Organic Fluorine in Molecular Crystals. *Cryst. Growth Des.* **2014**, *14*, 3155−3168.
(50) Mondal, P. K.; Yadav, H. R.; Roy Choudhury, A.; Chopra, D. Quantitative characterization of new supramolecular synthons involving fluorine atoms in the crystal structures of di-and

https://doi.org/10.1021/acs.cgd.1c00422
Cryst. Growth Des. 2021, 21, 4162−4177

tetrafluorinated benzamides. *Acta Crystallogr., Sect. B: Struct. Sci., Cryst. Eng. Mater.* **2017**, *73*, 805−819.
(51) Bhandary, S.; Gonde, S.; Chopra, D. Dissecting the Conformational and Interaction Topological Landscape of N-ethynylphenylbenzamide by the Device of Polymorphic Diversity. *Cryst. Growth Des.* **2019**, *19*, 1072−1085.
(52) Groom, C. R.; Bruno, I. J.; Lightfoot, M. P.; Ward, S. C. The Cambridge Structural Database. *Acta Crystallogr., Sect. B: Struct. Sci., Cryst. Eng. Mater.* **2016**, *B72*, 171−179.
(53) Berger, R.; Resnati, G.; Metrangolo, P.; Weber, E.; Hulliger, J. Organic fluorine compounds: a great opportunity for enhanced materials properties. *Chem. Soc. Rev.* **2011**, *40*, 3496−3508.
(54) Chopra, D.; Guru Row, T. N. Role of organic fluorine in crystal engineering. *CrystEngComm* **2011**, *13*, 2175−2186.
(55) Chopra, D. Is Organic Fluorine Really "Not" Polarizable? *Cryst. Growth Des.* **2012**, *12*, 541−546.
(56) Hathwar, V. R.; Chopra, D.; Panini, P.; Guru Row, T. N. Revealing the Polarizability of Organic Fluorine in the Trifluoromethyl Group: Implications in Supramolecular Chemistry. *Cryst. Growth Des.* **2014**, *14*, 5366−5369.
(57) Desiraju, G. R. Approaches to crystal structure landscape exploration. *Acta Crystallogr., Sect. B: Struct. Sci., Cryst. Eng. Mater.* **2017**, *73*, 775−778.
(58) Price, S. L. Predicting crystal structures of organic compounds. *Chem. Soc. Rev.* **2014**, *43*, 2098−2111.
(59) Thompson, H. P. G.; Day, G. M. Which conformations make stable crystal structures? Mapping crystalline molecular geometries to the conformational energy landscape. *Chem. Sci.* **2014**, *5*, 3173−3182.
(60) Dey, D.; Chopra, D. Evaluation of the Role of Isostructurality in Fluorinated Phenyl Benzoates. *Cryst. Growth Des.* **2017**, *17*, 5117−5128.
(61) Dey, D.; Chopra, D. Occurrence of 3D isostructurality in fluorinated phenyl benzamidines. *CrystEngComm* **2017**, *19*, 47−63.
(62) Mondal, P. K.; Chopra, D. Crystal structure landscape of conformationally flexible organo-fluorine compounds. *CrystEngComm* **2016**, *18*, 48−53.
(63) Bravais, A. *Etudes Cristallographiques*; Gauthier Villars: Paris, 1866.
(64) Friedel, G. Bravais Law Studies. *Bull. Soc. Fr. Mineral.* **1907**, *30*, 326−455.
(65) Donnay, J. D. H.; Harker, D. A new law of crystal morphology extending the Law of Bravais. *Am. Mineral.* **1937**, *22*, 446−467.
(66) Bernstein, J. *Polymorphism in Molecular Crystals*, 2nd ed.; Oxford University Press: Oxford, U.K., 2020.
(67) Kitaigorodskii, A. I. *Organic Chemical Crystallography*; Consultants Bureau: New York, 1961.
(68) Nelyubina, Y. V.; Glukhov, I. V.; Antipin, M. Y.; Lyssenko, K. A. Higher density does not mean higher stability" mystery of paracetamol finally unraveled. *Chem. Commun.* **2010**, *46*, 3469−3471.
(69) Gelbrich, T.; Hursthouse, M. B. Systematic investigation of the relationships between 25 crystal structures containing the carbamazepine molecule or a close analogue: a case study of the XPac method. *CrystEngComm* **2006**, *8*, 448−460.
(70) Gelbrich, T.; Hursthouse, M. B. A versatile procedure for the identification, description and quantification of structural similarity in molecular crystals. *CrystEngComm* **2005**, *7*, 324−336.
(71) Fabbiani, F. P. A.; Dittrich, B.; Florence, A. J.; Gelbrich, T.; Hursthouse, M. B.; Kuhs, W. F.; Shankland, N.; Sowa, H. Crystal structures with a challenge: high-pressure crystallisation of ciprofloxacin sodium salts and their recovery to ambient pressure. *CrystEngComm* **2009**, *11*, 1396−1406.
(72) Kalman, A.; Parkanyi, S.; Argay, G. Classification of the isostructurality of organic molecules in the crystalline state. *Acta Crystallogr., Sect. B: Struct. Sci.* **1993**, *B49*, 1039−1049.
(73) Fabian, L.; Kalman, A. Isostructurality in one and two dimensions: isostructurality of polymorphs. *Acta Crystallogr., Sect. B: Struct. Sci.* **2004**, *B60*, 547−558.
(74) Dey, D.; Chopra, D. Occurrence of 3D isostructurality in fluorinated phenyl benzamidines. *CrystEngComm* **2017**, *19*, 47−63.
(75) Esteves de Castro, R. A.; Canotilho, J.; Barbosa, R. M.; Silva, M. R.; Beja, A. M.; Paixao, J. A.; Redinha, J. S. Conformational Isomorphism of Organic Crystals: Racemic and Homochiral Atenolol. *Cryst. Growth Des.* **2007**, *7*, 496−500.
(76) Nath, K. N.; Nangia, A. Isomorphous Crystals by Chloro−Methyl Exchange in Polymorphic Fuchsones. *Cryst. Growth Des.* **2012**, *12*, 5411−5425.

https://doi.org/10.1021/acs.cgd.1c00422
Cryst. Growth Des. 2021, 21, 4162−4177